THE UNIVERSITY OF ALBERTA

EXTINCTION DISTANCE MEASUREMENTS IN SILICON

by

CARMAN DENNIS CANN

A THESIS

SUBMITTED TO THE FACULTY OF GRADUATE STUDIES

IN PARTIAL FULFILMENT OF THE REQUIREMENTS FOR THE

DEGREE OF MASTER OF SCIENCE

DEPARTMENT OF PHYSICS

EDMONTON, ALBERTA

JULY, 1967

UNIVERSITY OF ALBERTA

FACULTY OF GRADUATE STUDIES

The undersigned certify that they have read, and recommend to the Faculty of Graduate Studies for acceptance, a thesis entitled "EXTINCTION DISTANCE MEASUREMENTS IN SILICON", submitted by Carman Dennis Cann in partial fulfilment of the requirements for the degree of Master of Science.

ABSTRACT

Extinction distance measurements provide a method of testing the predictions of the dynamical theory of electron diffraction.

Using silicon as the specimen material, we have made measurements of the variation of the (111) and (220) extinction distances with the angular deviation of these reflections from their Bragg orientations. The (220) measurements showed good agreement with both the two-beam and, taking into account systematic reflections, multi-beam approximations of the dynamical theory. However, the (111) results were in poor agreement with the two-beam approximation and only in qualitative agreement with the multi-beam approximation. Better agreement was found with a multi-beam approximation in which an experimental value of 2.83 A for the (111) electron scattering factor was used. This value was calculated from the value of 840 $\pm$ 40A measured here for the (111) extinction distance at 152 kV. These latter calculations are in good agreement with recent measurements of the corresponding X-ray scattering factor.

ACKNOWLEDGEMENTS

I wish to express my sincere gratitude to Dr. S.S. Sheinin, my research supervisor, both for suggesting this project and for his encouragement and patience throughout the course of this work.

I wish to thank Mr. J.C. Brunel for his very capable assistance with the technical problems involved with the preparation of specimens and the analysing of results.

Thanks are also due the other technical staff of the Physics Department for their assistance in preparing some of the apparatus used in these experiments.

I also wish to express my thanks to Mr. Charles Elliott for his assistance in writing the computer programs and to the staff of the Computing Centre for making their facilities available to me.

For typing done during the initial preparation of this manuscript I wish to thank Miss R. Borton.

For the final typing of the manuscript I would like to express my sincere appreciation to Mrs. L. Medford.

Finally, I would like to express my thanks to the National Research Council for financial support throughout the course of this project.

TABLE OF CONTENTS

LIST OF FIGURES

CHAPTER I

INTRODUCTION

The interpretation of the results of electron diffraction experiments depends on the type of interaction the incident electrons are assumed to have with the target material. Until the perfection of the electron microscope[1], electron diffraction results were usually interpreted in terms of the kinematical theory of electron diffraction which is similar in its approach to the theory commonly used in X-ray diffraction. However, electron microscope images of wedge-shaped crystalline materials obtained in the early 1940's[2-7] had intensity variations which could only partially be explained by this theory. These variations, known as thickness extinction contours were similar to those shown in Figure 1. The kinematical theory was able to account for these observations by predicting that the diffracted beam would vary periodically with depth in the crystal. As shown in Figure 2, this periodicity would result in the presence of extinction contours in dark field electron micrographs of wedge-shaped crystals. However, the kinematical theory also predicts that the period of this variation or the extinction distance becomes infinite as the diffracted beam approaches the Bragg condition. This was in disagreement with experimental observations[2-7] that the extinction distance remained finite. Because of the failure of the

Figure 1

Dark field image of a silicon crystal showing the presence of extinction contours in wedge-shaped regions. x 20,000

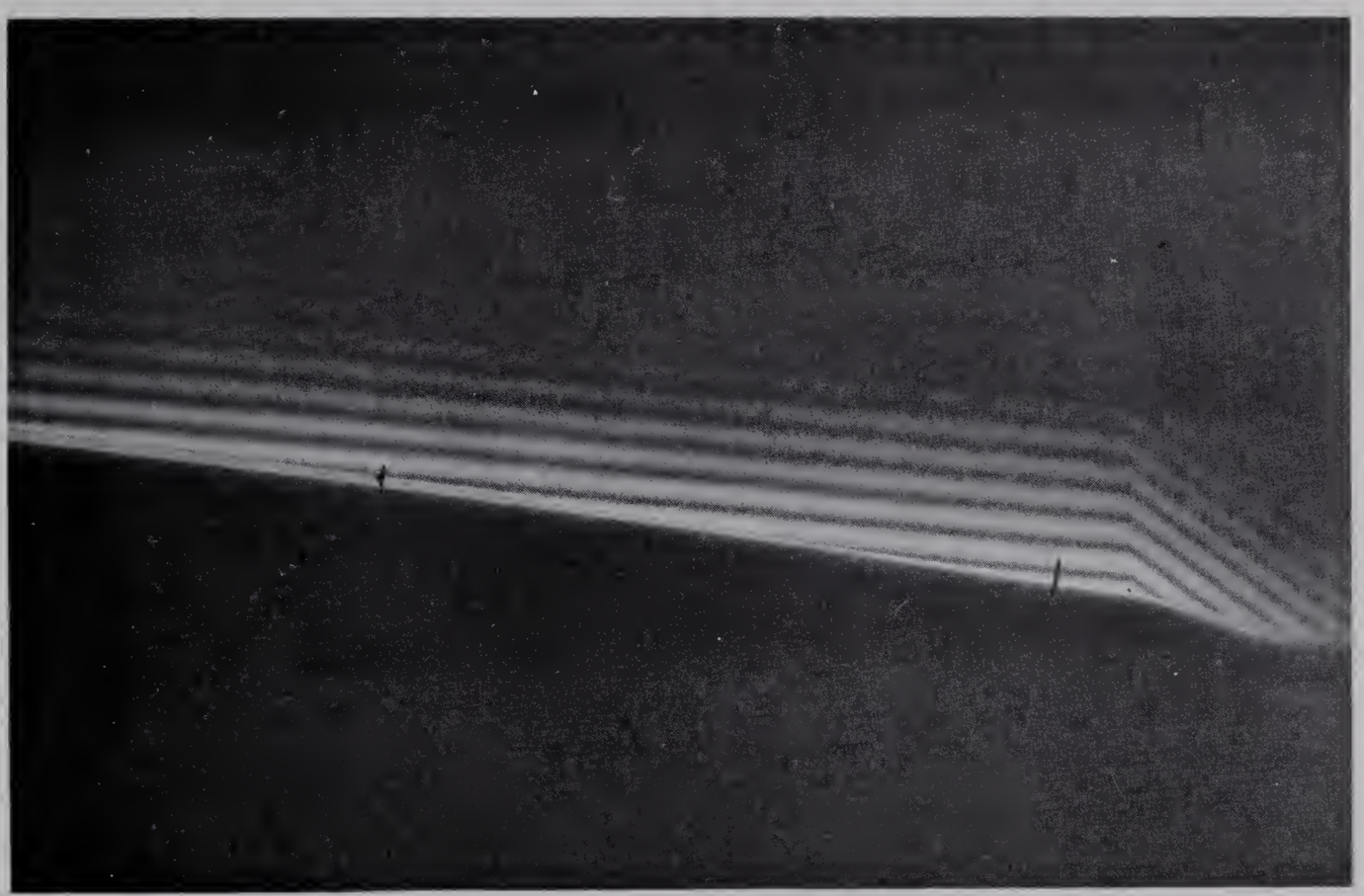

Figure 2

A schematic illustration showing the origin of extinction contours (a) Cross section of a wedge-shaped crystal showing the depth periodicity of I_g, the intensity of a diffracted beam. ξ is the extinction distance. The arrow points in the direction of the incident beam. (b) The dark field image of the crystal with extinction contours at positions E

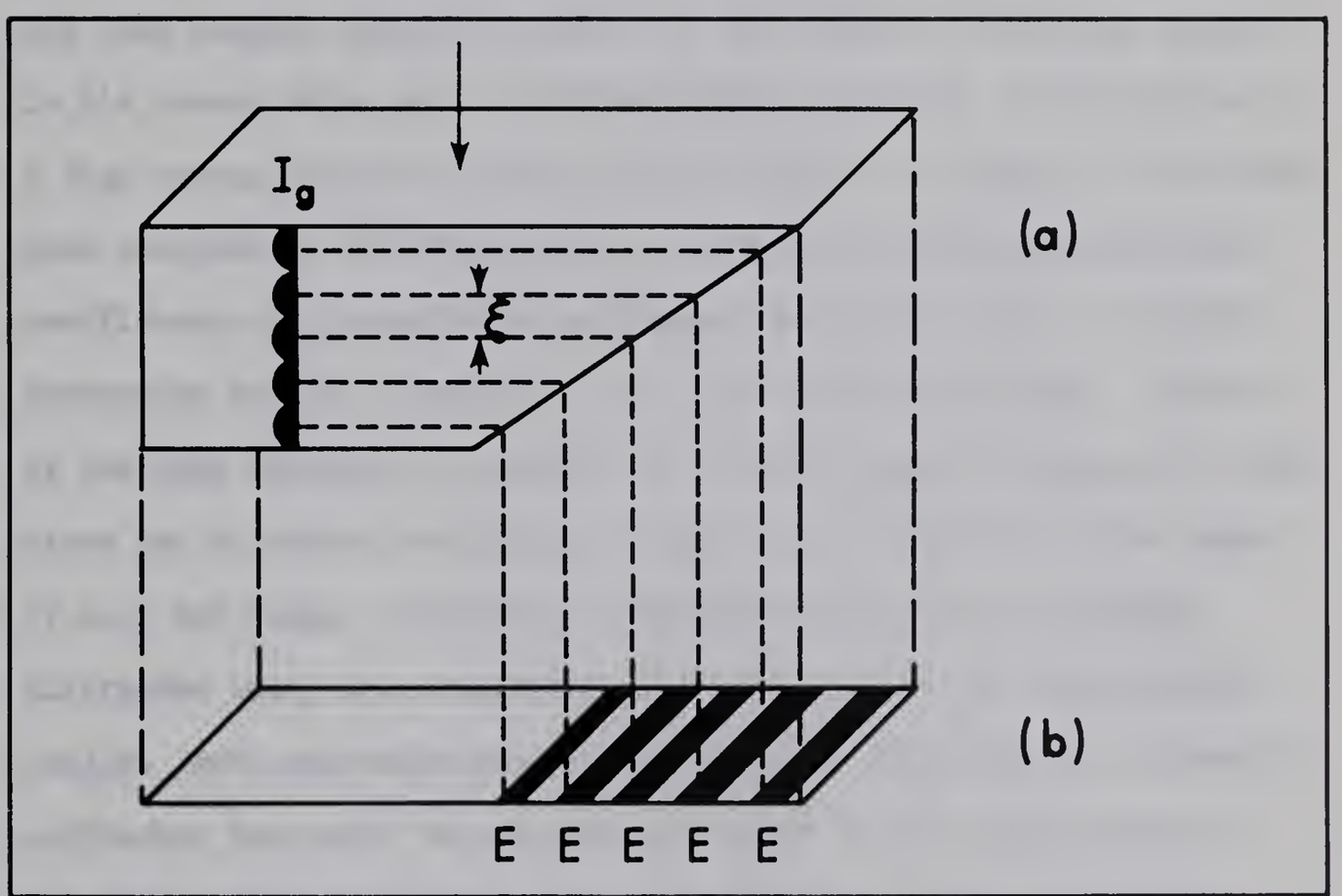

FIGURE 2

ANEXO 3

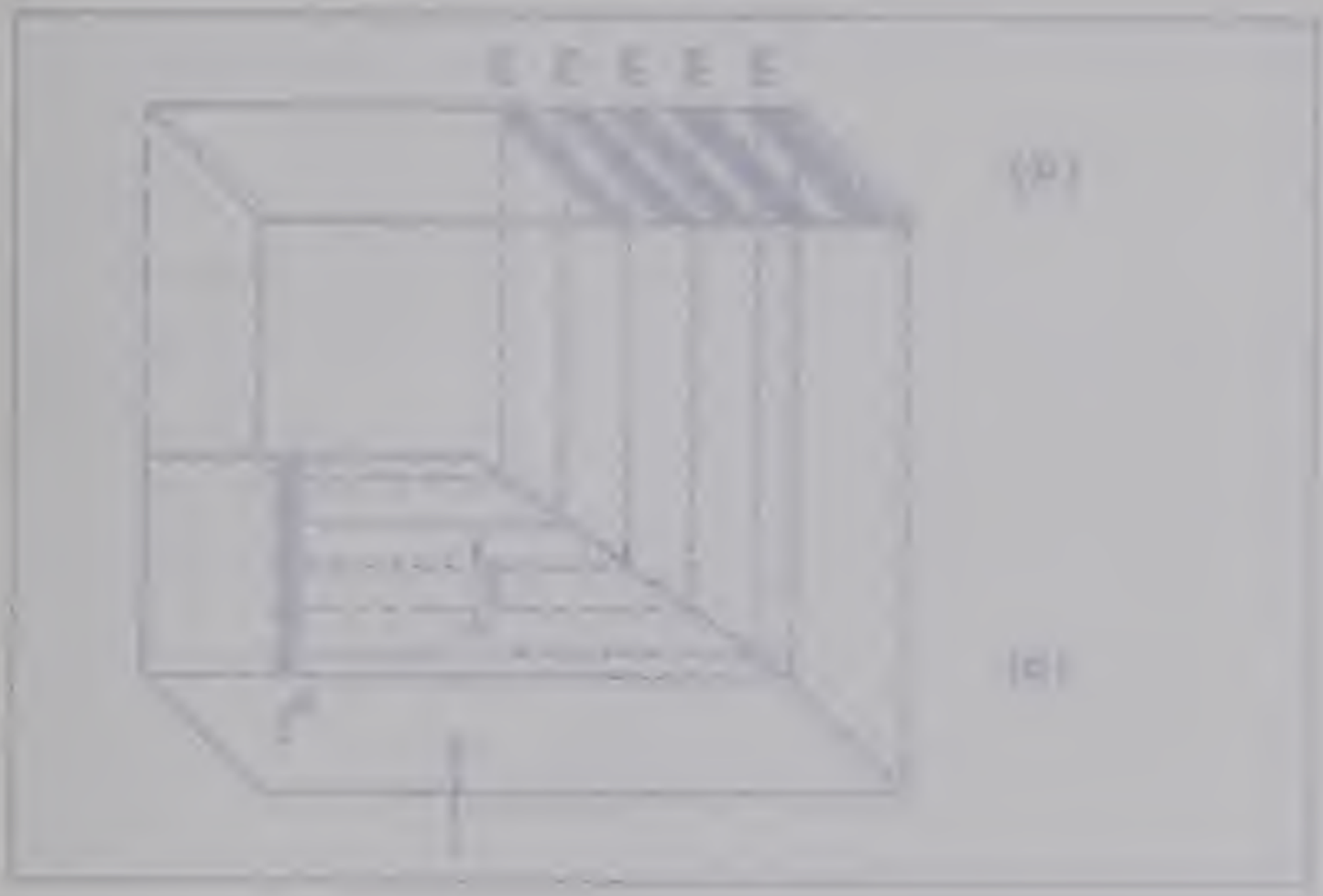

kinematical theory near the Bragg orientation, experimenters turned to the dynamical theory of electron diffraction in order to interpret their results.

The dynamical theory had been proposed by Bethe[8] in 1929 but had been largely ignored in favour of the simpler kinematical theory. In his theory Bethe gave a wave mechanical treatment of the motion of a high energy electron in the periodic field of a crystal. This treatment resulted in an infinite set of equations relating the amplitude coefficients of the different diffracted beams and, thus, no general expression for the intensity of an image could be obtained. However, if the same treatment is applied to a finite number of beams, the equations can be solved numerically to give the intensities of the beams. If only two beams, the directly transmitted beam and one strongly diffracted beam, are considered, the equations can be solved analytically. Both approximations predict that the intensity of a strongly diffracted beam will be periodic with depth in the crystal even at the exact Bragg condition. Thus, the dynamical theory can explain, at least qualitatively, the aforementioned experimental results.[2-7]

The dynamical theory predicts, further, that the extinction distance of a diffracted beam is dependent on both the energy of the incident electrons and $\Delta\theta$, the angular deviation of the crystal from the exact Bragg orientation for that reflection. Relatively little work, however, has been done to test these predictions quantitatively.

The energy dependence has been examined by only two groups. Hashimoto[9] measured the variation of extinction distance in aluminum foils with electron energy for accelerating voltages from 50 to 300 kV and found that the experimental results agreed very well with the theoretical two-beam predictions. However, Dupouy[10] et al. in taking similar measurements on MgO in the range from 100 to 1000 kV found significant deviations from the two-beam predictions, especially at the higher accelerating voltages. Goringe et al.[11] showed that these deviations could be explained by taking into account systematic reflections by means of the multi-beam dynamical theory. The dependence of extinction distance on $\Delta\theta$ has been investigated by only one group. Uyeda and Nonoyama[12] measured the variation of extinction distance with angular deviation from the exact Bragg orientation for the (200) reflection in MgO wedge-shaped crystals and found good agreement with the theory. Their results were obtained at random $\Delta\theta$'s as determined by measurements from electron diffraction patterns. However, such determinations are of only moderate accuracy, a fact which becomes very important when small $\Delta\theta$'s are considered.

Because of the limited amount of work that has been done, further experiments to test the predictions of the dynamical theory were proposed. The purpose of the experiments was to investigate in a systematic and accurate manner the $\Delta\theta$ dependence of extinction distance and to compare the results with the predictions of the two-beam

and multi-beam dynamical theories of electron diffraction. It is a report of this work that forms the basis of this thesis.

CHAPTER II

DYNAMICAL THEORY OF ELECTRON DIFFRACTION

The dynamical theory of electron diffraction as first proposed by Bethe[8] and further developed by MacGillavry[13] and Heidenreich[14] starts with the Schroedinger equation for an electron in a crystal potential $V(\bar{r})$. This equation can be written

$$\nabla^2\psi(r) + \left(\frac{8\pi^2 me}{h^2}\right)\Big(E + V(r)\Big)\psi(r) = 0,$$

where $\psi(r)$ is the wave function of the electron, $\bar{r}$ is the position vector, m and e are the rest mass and charge of the electron, E is the potential through which the electron was accelerated before entering the crystal and h is Planck's constant. Due to the periodic nature of the crystal potential, $V(\bar{r})$ can be expressed by a Fourier series

$$V(\bar{r}) = v_o + \sum_{\bar{g}}{}' v_g e^{2\pi i(\bar{g}\cdot\bar{r})},$$

where v_o is the mean inner potential, $\bar{g}$ is a reciprocal lattice vector, v_g is the g'th coefficient of the lattice potential and the prime means that the term $\bar{g} = 0$ is excluded from the summation. Through the use of Poisson's equation and X-ray scattering factors, the Fourier coefficients of the lattice potential can be found in terms of electron

scattering factors. The expression is[15]

$$V_g = \frac{47.87}{\Omega} \sum_j f_j(s) e^{-2\pi i (\bar{g} \cdot \bar{r}_j)} \text{ volts},$$

where 47.87 is a numerical value resulting from the evaluation of physical constants, Ω is the volume of the unit cell in A^3 and $f_j(s)$ is the electron scattering factor in A of the j'th atom in the unit cell. The parameter s is equal to $4\pi \sin \theta/\lambda$ where 2θ is the scattering angle and λ is the wavelength of the incident electrons.

In the case of electrons with energies of the order of those usually used in electron microscopes, E is much greater than $V(\bar{r})$ and the Schroedinger equation can be solved using a perturbation approach. The solutions of the equation outside the crystal where $V(\bar{r}) = 0$ are plane waves of the form

$$\psi(r) = \exp(2\pi i \bar{\chi} \cdot \bar{r}),$$

where the magnitude of the wave vector $\bar{\chi}$ is such that

$$\frac{h^2 \chi^2}{2m} = eE$$

The effect of the lattice potential is to give solutions of the Schroedinger equation which are combinations of free electron plane waves. Since the potential is periodic, the solutions must be Bloch

functions. Thus, they are of the form

$$\psi(\bar{r}) = \sum_{\bar{g}} C_{\bar{g}}(\bar{k}) e^{2\pi i (\bar{k}_g \cdot \bar{r})}$$

where $\bar{k}_g = \bar{k} + \bar{g}$. $\bar{k}$ is the wave vector in the crystal in the direction of the directly transmitted wave. These expressions for $V(\bar{r})$ and $\psi(\bar{r})$ are then substituted into the Schroedinger equation to obtain

$$\sum_{\bar{g}} \left[- k_g^2 C_g(\bar{k}) + \frac{2me}{h^2}\left[E + v_o\right] C_g(\bar{k}) + \frac{2me}{h^2} \sum_{\bar{h}}{}' C_{g-h}(\bar{k}) v_h \right] e^{2\pi i (\bar{k}_g \cdot \bar{r})} = 0,$$

where the prime on the second summation means the term $\bar{h} = 0$ is omitted. Since the $e^{2\pi i (\bar{k}_g \cdot \bar{r})}$ are linearly independent, the coefficients of these exponentials must all equal zero. This condition results in a set of equations of the form

$$(K^2 - k_g^2) C_g(\bar{k}) + \sum_{\bar{h}}{}' U_h C_{g-h}(\bar{k}) = 0 \qquad (1)$$

where $K = \frac{2me}{h^2}(E + v_o)$ and $U_g = \frac{2me}{h^2} v_g$.

This set of equations, called the "dispersion equation" by Bethe[8], gives the general relations between the amplitude coefficients C_g, the Fourier coefficient terms U_g, and the wave vectors of the electrons $\bar{k}_g$. It is from these relations that the approximate solutions of the dynamical theory are developed.

A. Two-Beam Approximation

In the two-beam approximation only the transmitted beam $\bar{k}$ and one diffracted beam $\bar{k}_g$ are considered. In this case the set of equations reduces to

$$(K^2 - k^2)C_o(\bar{k}) + U_{-g}C_g(\bar{k}) = 0$$

$$(K^2 - k_g^2)C_g(\bar{k}) + U_g C_o(\bar{k}) = 0$$

Since the potential energy of the lattice must be real

$$U_g = U_{-g}^*$$

Also, since the type of crystal in which we are interested is centro-symmetric

$$U_g = U_{-g}$$

Therefore, the constant U_g is real. Now, non-zero solutions exist for $C_o(\bar{k})$ and $C_g(\bar{k})$ only if the determinant formed by the coefficients vanishes, i.e. if

$$(K^2 - k^2)(K^2 - k_g^2) - U_g^2 = 0$$

Since K and k are nearly equal and much larger than g in magnitude, this equation can be rewritten as

$$(k - K)(k_g - K) = \frac{U_g^2}{4K^2}$$

The values of k satisfying this equation lie on a surface in k-space called the dispersion surface (see Figure 3). Physically, the theory predicts that a degenerate energy level corresponding to energy $\frac{h^2K^2}{2m}$ is split by the perturbing potential into two new levels, one slightly below and one slightly above the old level. An electron in the crystal with wave vector K is thus scattered into two new states with wave vectors $k^{(1)}$ and $k^{(2)}$. These states have the same total energy but different kinetic energies.

In order to find the amplitude of the diffracted beam at the exit surface of the crystal, the boundary conditions at the entrance and exit surfaces must be considered. Since the energy of the electrons is much greater than the potential energy of the lattice, reflected waves from the two surfaces can be ignored. The boundary conditions then reduce to simple continuity of transmitted and diffracted wave amplitudes at the surfaces. Thus, the amplitude of any beam just outside a surface is equal to the sum, taking into account phase differences, of the amplitudes of the Bloch wave components in the direction of that beam in the crystal.

These boundary conditions result in an expression for the amplitude of the diffracted beam which is proportional to the difference of two exponentials. If the surfaces of the crystal lie approximately parallel to the xy plane and the beam traverses it in the negative z direction, this difference term can be written

Figure 3

The dispersion surface in the two-beam approximation. $D^{(1)}$ and $D^{(2)}$ are the lower and upper branches of the surface respectively. In this drawing $\gamma^{(1)} = EH$, $\gamma^{(2)} = FE$, and $U_g/2K = AB = BC$.

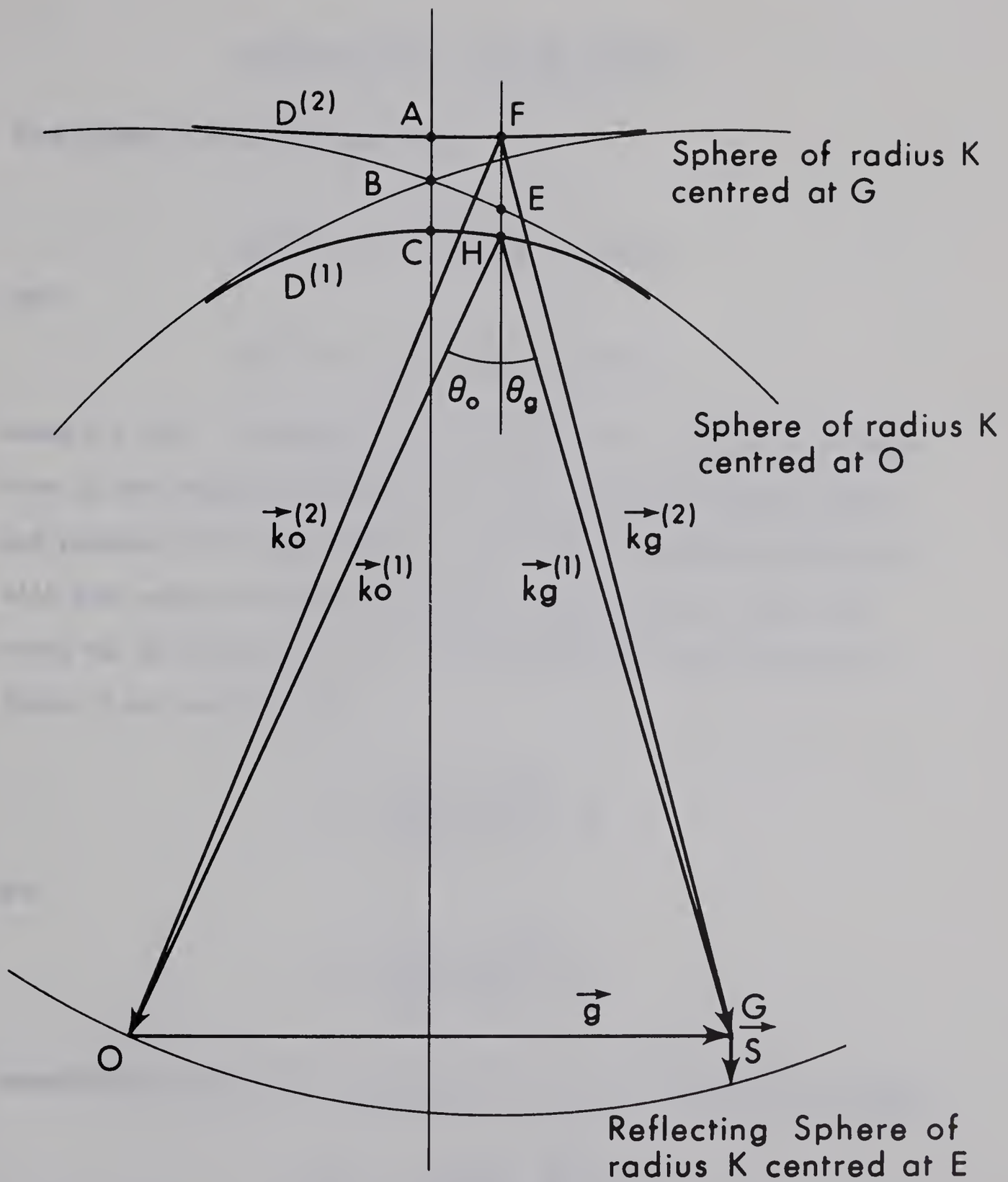
D(2)
A
F
Sphere of radius K
centred at G
B
E
C
H
D(1)
θo
θg
Sphere of radius K
centred at O
k(2)o
k(1)o
k(1)g
k(2)g
g
G
S
O
Reflecting Sphere of
radius K centred at E

FIGURE 3

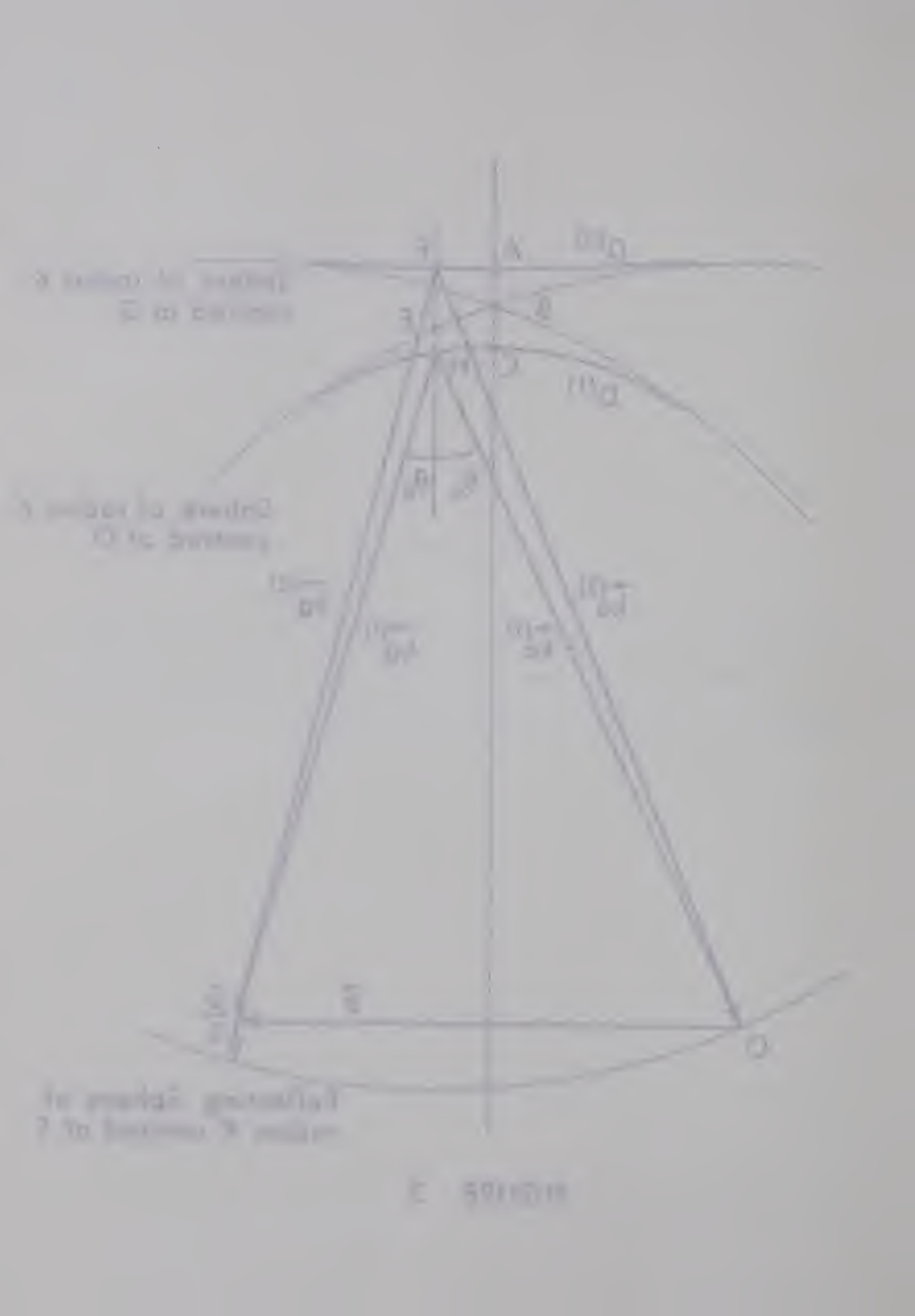

$$\exp(2\pi i k_g^{(2)} z) - \exp(2\pi i k_g^{(1)} z)$$

From Figure 3 it can be seen that

$$k_g^{(1)} = K - \gamma^{(1)} \cos\theta_g - s \cos\theta_g$$

and

$$k_g^{(2)} = K + \gamma^{(2)} \cos\theta_g - s \cos\theta_g$$

where $\bar{s} = \bar{g}\Delta\theta$. The general sign convention for s is that s is negative if the reciprocal lattice point lies outside the Ewald sphere and positive if it lies inside. In the case of electron diffraction with high energy electrons $|K| \gg |g|$ so that θ_g is very small and $\cos\theta_g$ can be set equal to one. From geometrical considerations in Figure 3, one can show that

$$\gamma^{(1)} = \left(\frac{U_g^2}{4K^2} + \frac{s^2}{4}\right)^{\frac{1}{2}} - \frac{s}{2}$$

and

$$\gamma^{(2)} = \left(\frac{U_g^2}{4K^2} + \frac{s^2}{4}\right)^{\frac{1}{2}} + \frac{s}{2}$$

Substituting these into the expressions for $k_g^{(1)}$ and $k_g^{(2)}$ we obtain

$$k_g^{(1)} = K - \left(\frac{U_g^2}{4K} + \frac{s^2}{4}\right)^{\frac{1}{2}} - \frac{s}{2}$$

and

$$k_g^{(2)} = K + \left(\frac{U_g^2}{4K} + \frac{s^2}{4}\right)^{\frac{1}{2}} - \frac{s}{2}$$

When these expressions for $k_g^{(1)}$ and $k_g^{(2)}$ are substituted into the exponential difference factor, the amplitude is found to be proportional to

$$\exp\left[2\pi i\,(K - \frac{s}{2})z\right]\sin\left[\pi z(\frac{U_g^2}{K^2} + s^2)\right]$$

or I_g, the intensity of the diffracted beam is proportional to

$$\sin^2\left[\pi z(\frac{U_g^2}{K^2} + s^2)^{\frac{1}{2}}\right]$$

At the exact Bragg condition s = 0 and the extinction distance, ξ_o, equals K/U_g. ξ, the extinction distance when s is not equal to zero, can be written in terms of ξ_o in the form

$$\xi = \xi_o(1 + \frac{s^2K^2}{U_g^2})^{-\frac{1}{2}}$$

or

$$\xi/\xi_o = 1/(1 + \frac{s^2K^2}{U_g^2})^{\frac{1}{2}}$$

This last expression gives the variation of extinction distance with

angular deviation from the exact Bragg condition as predicted by the two-beam dynamical theory of electron diffraction.

B. Multi-Beam Approximation

In the case where n beams are taken into consideration several authors[16-19] have proposed scattering matrix formulations of the theory. The formulation proposed by Howie and Whelan[17] gives the most exact numerical solutions. It starts at (1), the dispersion equation. If the determinant of the coefficients of the amplitudes is set equal to zero, an equation of degree n in k results. The solutions to this equation define n dispersion surfaces in k-space. Then, by analogy with the two-beam case, for the i'th dispersion surface

$$K^2 - k^{(i)^2} = -2K\gamma^{(i)}$$

and

$$K^2 - k_g^{(i)^2} = 2K(s_g - \gamma^{(i)})$$

Substitution of these expressions into (1) results in an eigenvalue equation of the form

$$\underline{A}\bar{C}^{(i)} = \gamma^{(i)}\bar{C}^{(i)}, \qquad (2)$$

where $\bar{C}^{(i)}$ is a column vector whose elements, $C_g^{(i)}$, are the wave amplitudes of a Block wave, $\gamma^{(i)}$ is the corresponding value of γ and $\underline{A}$ is a

matrix whose elements are $A_{oo} = 0$, $A_{gg} = s_g$ and $A_{gh} = U_{g-h}/2K$ where $g \neq h$.

Consider now the situation shown in Figure 4. Waves in the directions of the n beams being considered, are incident upon a slab of crystal of thickness δz. These waves can be represented by a column vector $\bar{u}$ whose components are the amplitudes of the various waves. The boundary conditions at the upper surface of the slab result in a set of equations of the form

$$\sum_i \psi^{(i)} C_g^{(i)} = u_g$$

or, in matrix notation

$$\underline{C}\bar{\Psi} = \bar{u},$$

where $\underline{C}$ is a matrix whose columns are the eigenvectors of (2) and $\bar{\Psi}$ is a column vector whose elements give the excitation of the Bloch waves on the various branches of the dispersion surface. $\bar{\Psi}$ can be found from the equation

$$\bar{\Psi} = \underline{C}^{-1}\bar{u} = \underline{\tilde{C}}\bar{u}$$

since $\underline{C}$ is an orthogonal matrix. The boundary conditions at the bottom surface of the slab are, taking into account phase differences of waves from different dispersion surfaces

$$u_g' = \sum_i \psi^{(i)} C_g^{(i)} \exp(2\pi i \gamma^{(i)} \delta z)$$

Figure 4

Waves propagating through a thin slab of crystal

(From Howie and Whelan[17])

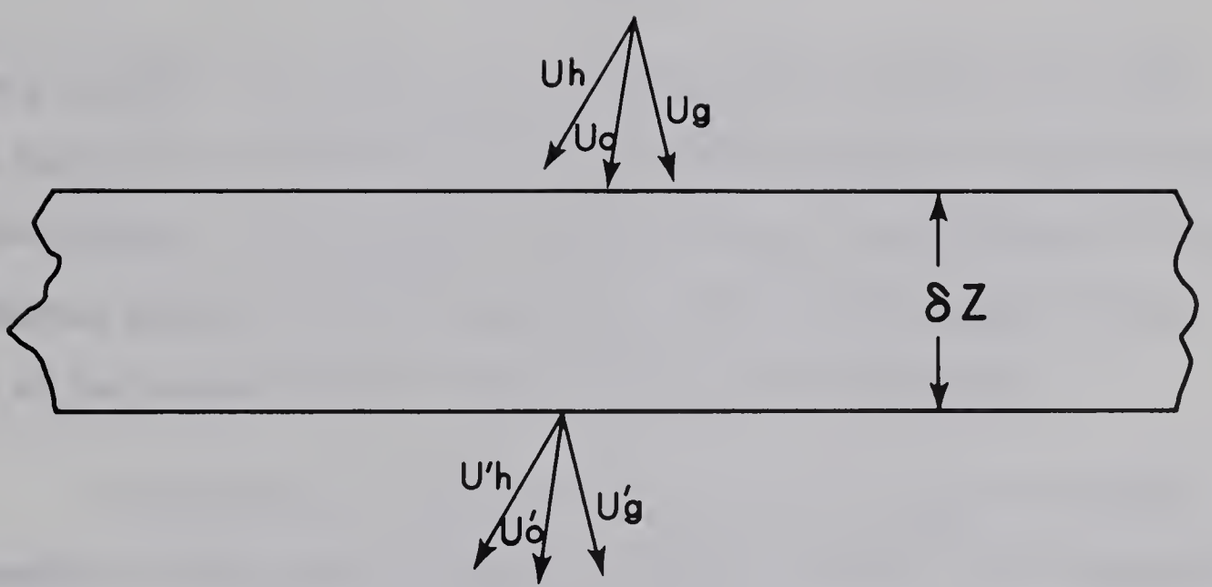

FIGURE 4

or, in matrix form

$$\bar{u}' = \underline{C\gamma}\bar{\psi},$$

where $\underline{\gamma}$ is a diagonal matrix whose components are $\exp(2\pi i \gamma^{(i)}\delta z)$. Substituting for $\bar{\psi}$ with the expression we obtained above, we have

$$\bar{u}' = \underline{P}\bar{u},$$

where $\underline{P} = \underline{C\gamma C}^{-1}$. $\underline{P}$ is, thus, a scattering matrix relating the amplitude vectors $\bar{u}'$ at the bottom surface to the incident wave $\bar{u}$ at the top of the crystal. For any finite number of beams, the components of the scattering matrix $\underline{P}$ can be computed and, thus, the intensity of any beam at the bottom surface of the crystal can be determined.

The theories as outlined so far have not taken into account absorption or relativistic effects. Hashimoto *et al.*[20] have considered absorption in the two-beam case by assuming a complex lattice potential. Their calculations predict that the only effect of the absorption will be a decrease in intensity but no change in extinction distance. There have been no published calculations on the effect of absorption on extinction distance in the multi-beam case. However, preliminary results of calculations being currently carried out in this laboratory predict that when only two strong beams are present any corrections to the extinction distance would be second-order in magnitude. Because many electron microscopes have accelerating voltages of 80 kV or higher, relativistic effects must be taken into consideration.

Fujiwara[21] developed a relativistic dynamical theory of electron diffraction using the Dirac wave equation. His results show that the non-relativistic theory developed using the Schroedinger wave equation can be corrected for relativistic effects by two simple substitutions. These are the replacing of the non-relativistic wavelength by a relativistically corrected one and by multiplying the Fourier coefficient term U_g by β where

$$\beta = \left(1 - \frac{v^2}{c^2}\right)^{-\frac{1}{2}}.$$

Here v and c are the velocities of the electrons and light respectively.

CHAPTER III

EXPERIMENTAL TECHNIQUE

Two different experiments have been proposed to test the predictions of the two-beam and multi-beam approximations of the dynamical theory. The first of these involved the measurement of changes in the spacing of extinction contours resulting from the systematic variation of the orientation of a wedge-shaped crystal. From such measurements the variation of ξ/ξ_o with $\Delta\theta$ can be determined. The second proposal was to measure the actual spacing of extinction contours in the images of wedge-shaped crystals of known wedge angle. From this spacing, the magnification of the image, and the wedge angle of the crystal, values of ξ_o can be determined. It was decided to carry out these experiments using the $\{111\}$ and $\{220\}$ reflections in silicon at electron microscope accelerating voltages of 100 and 152 kV.

The actual procedure in making these measurements can be divided into four parts. These are calibration measurements, specimen preparation, electron microscope examination, and analysis of observations.

A. Calibration Measurements

The extinction distance measurements were carried out in a

JEM 150 electron microscope using a tilting-rotating stage to vary the orientation of the crystal specimen. This stage allowed the specimen to be tilted through a range of $\pm 10^{o}$ about an axis perpendicular to the incident electron beam and rotated through 360^{o} about an axis perpendicular to the plane of the specimen. In order to be able to tilt the specimen through a known angle, a high precision click-type control that allowed the angle of tilt to be changed in increments of 0.025^{o} was used.

(i) Tilt Axis Direction Determination

In the ξ/ξ_{o} versus $\Delta\theta$ measurements, the specimen was oriented so that the set of planes, corresponding to a reflection of interest, were parallel to the axis of tilt of the stage. In this orientation, a given change in the angle of tilt of the specimen results in an equal change in the value of $\Delta\theta$. However, in order to orient the specimen in this manner, the direction of the axis of tilt, as seen at the viewing screen of the microscope, had to be determined. This was done by using the fact that, as the specimen is tilted, the Kikuchi pattern must move in a direction perpendicular to the tilting axis of the stage. The direction of this motion was found by taking a series of electron micrographs of the diffraction pattern of the specimen as it was being tilted. The Kikuchi patterns in these micrographs were then examined and the direction of motion determined from the direction of shift of

the patterns in the micrographs. This method of determination allowed the direction of the axis of tilt as seen at the viewing screen to be found within $\pm 3^{\circ}$. It should be noted that this direction is not the same as the actual tilt axis direction in the stage due to rotation of the image in the magnetic lenses of the microscope.

(ii) Tilt Calibration

The precision with which $\Delta\theta$ can be found depends on the accuracy with which the specimen can be tilted. The specimen tilting system was checked for both long range errors, which would result in the average increment of tilt being different than the designed $.025^{\circ}$, and short range errors which would result in random variations of the increment. The long range errors were found by tilting the specimen through a known angle as determined from the initial and final Kikuchi patterns and comparing this angle with the angle of tilt as determined from the tilt control.

In an actual check the specimen was oriented so that a row of systematic reflections was perpendicular to the tilt axis direction. The specimen was then tilted from an orientation in which the (hkl) reflection was in the Bragg condition to one in which the $(\bar{h}\bar{k}\bar{l})$ reflection was in the Bragg condition (see Figure 5). The exact Bragg orientation for a reflection was determined from the fact that, under these conditions, a bright Kikuchi line must pass through the middle

of the spot. Tilting the specimen in this manner results in the orientation of the specimen being changed by an angle equal to twice the Bragg angle of the (hkl) reflection. The angle through which the specimen was tilted as given by the tilt control was then compared with this angle to determine the accuracy of the tilting mechanism. After carrying out this check over different parts of the range of tilt of the stage, it was found that the angles of tilt as given by the tilt control were within one per cent of those determined from Kikuchi patterns.

The short range random variations in increment size were checked by using a method given by Sheinin[22]. In general they were found to be less than 10 per cent of the increment size although occasional variations ranging up to 50 per cent were noted. However, these variations usually occurred in pairs in such a manner that the average increment found from the two of them would still be approximately $.025^{\circ}$. Moreover, such variations would result in scatter in the results of a size which is already, in general, less than the range allowed for the experimental points (see Figures 10, 11, 12 and 13).

The accuracy of the rotation control of the stage was not checked as precise rotations of the specimen were not required.

Figure 5

A drawing of a diffraction pattern showing the initial and final orientations in the accuracy check of the stage. The arrow shows the direction of the tilt axis.

(a) Initial orientation showing the bright (hkl) Kikuchi line passing directly through the (hkl) spot.

(b) Final orientation showing the bright ($\bar{h}\bar{k}\bar{l}$) Kikuchi line passing directly through the ($\bar{h}\bar{k}\bar{l}$) spot

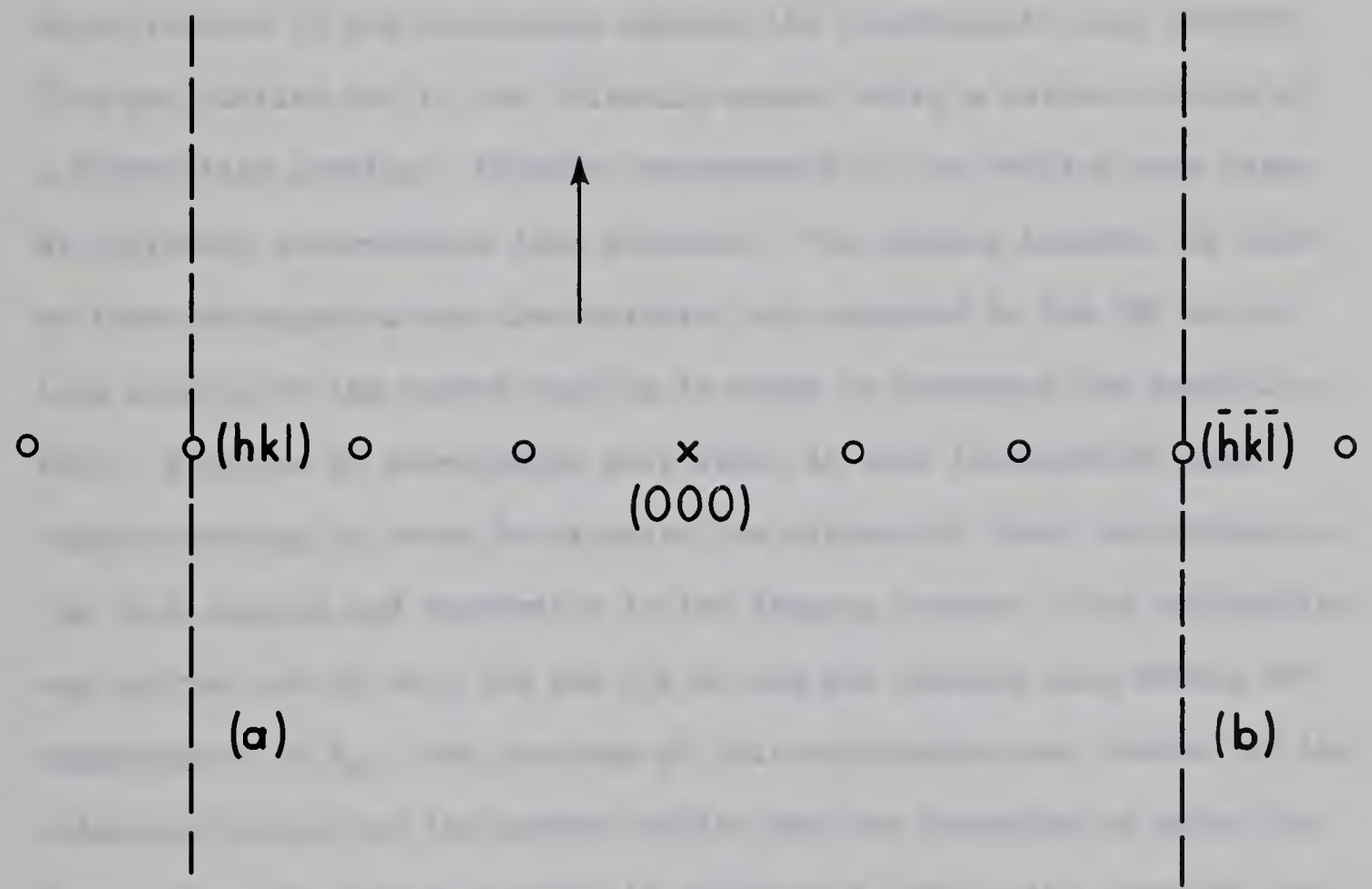

FIGURE 5

(iii) Magnification Calibration

In measuring ξ_o it was necessary to know the magnification of the images. This magnification is controlled by the current in the intermediate lens of the microscope. Thus, in order to know the magnification of the image it was necessary to accurately calibrate the magnification of the microscope against the intermediate lens current. This was carried out in the following manner using a carbon replica of a diffraction grating. Electron micrographs of the replica were taken at different intermediate lens currents. The spacing between the lines on these micrographs was then measured and compared to the 882 mμ per line spacing of the carbon replica in order to determine the magnification. A series of micrographs were taken at each intermediate lens current setting in order to minimize the effects of local variations in the line spacing and distortion in the imaging system. This calibration was carried out at both 100 and 152 kV and was checked once during the measurements of ξ_o. The accuracy of this calibration was limited by the tolerance quoted for the carbon replica and the precision to which the intermediate lens current could be determined. These two combined gave a possible error of $\pm$ 3 per cent to the calibration curve.

B. Specimen Preparation

In order to make precise extinction distance measurements, smooth regular wedge-shaped specimens containing no strains were

required. Silicon was chosen as the material from which to prepare such specimens for two reasons. Firstly, a technique was available to grow needle-shaped crystals or whiskers which had the necessary wedge shape and, secondly, the natural brittleness of silicon helped to prevent the formation of strains in these specimens.

The technique used to grow the whiskers involved the disproportionation of SiI_2. The actual experimental method employed was similar to that used by other researchers [23-25]. In a typical run the following procedure was carried out. A piece of clear quartz tubing (25 cm in length and about 140 cm^3 in volume) was sealed at one end and the following quantities of high purity chemicals put into it: 0.84 g of iodine, 1 g of silicon, and 2 to 3 mg of nickel. The tube was then evacuated to a pressure of about 5×10^{-6} Torr and sealed off. In order to prevent the loss of iodine into the evacuating system at such low pressures, the end of the tube containing the chemicals was immersed in liquid nitrogen during the evacuation process. The sealed tube was then put in a horizontal cylindrical furnace whose operating temperature varied smoothly from 1150° C at one end to 800° C at the other. The chemicals in the tube were located in the hotter region of the furnace. After about two hours, the tube was withdrawn and allowed to cool. Inside of it could be seen whiskers ranging in size from about a centimeter long and a millimeter in diameter down to very fine filaments less than a micron in diameter. The size of the whiskers

appeared to depend on the temperature of the region in which they grew with the larger whiskers being located in the hotter regions. After it had cooled, the tube was broken open and the whiskers collected. The process involved in the growth of the crystals has been studied[26,27] and found to be a thermochemical one using the disproportionation reaction:

$$2SiI_2(g) \rightleftharpoons Si(s) + SiI_4(g)$$

At temperatures in the range of 1100° C the reaction moves to the left while at temperatures in the range of 950° C the reaction moves to the right. Thus, in the furnace this reaction results in a net transport of silicon from the hot region to the cooler regions of the tube. Under the conditions described above, the Si comes out of the SiI_2 compound in the form of needle-shaped crystals. It was found[25] that the addition of a small amount of impurity such as gold or nickel greatly increased the probability of formation of such crystals.

C. Electron Microscope Examination

The determinations of extinction distance parameters were made from observations made in the electron microscope. The actual process used in making these observations consisted of choosing and orienting a suitable specimen and then taking a series of electron micrographs as the specimen was systematically tilted. However, the choice of a suitable specimen, how it oriented and how the micrographs

were taken depended on the type of measurement being made.

(i) Measurements of $\mathcal{E}/\mathcal{E}_o$ Versus $\Delta\theta$

A specimen suitable for making this type of measurement was chosen in the following way. First, it had to be a strain free region of uniform thin wedge-shaped single crystal. Thin wedges were required so that the extinction contours could still be resolved at large values of $\Delta\theta$ where $\mathcal{E}$ is quite small. Then, a diffraction pattern of this region had to contain at least one of the two reflections of interest. If it did, the specimen was then oriented so that the set of planes corresponding to this reflection were parallel to the axis of tilt of the stage. If the only strong low-order reflections then present in the diffraction pattern were in the row of systematic reflections corresponding to this set of planes, the specimen was used for making measurements of $\mathcal{E}/\mathcal{E}_o$. This last feature was required because one of the purposes of this experiment was to test the predictions of the two-beam dynamical theory. The closest approximation to a two-beam situation achievable in a real crystal is that in which only a single row of systematic reflections is present in the diffraction pattern. This is difficult to achieve in practice so specimens whose diffraction patterns contained high-order spots off the row were also used. Suitable regions having all the necessary qualifications were usually found at the intersection of two whiskers (see Figure 6).

Figure 6

An electron micrograph showing the type of crystal formation in which suitable regions for $\varepsilon/\varepsilon_o$ versus $\Delta\theta$ measurements were found. Smaller filament type whiskers are also visible. x 500

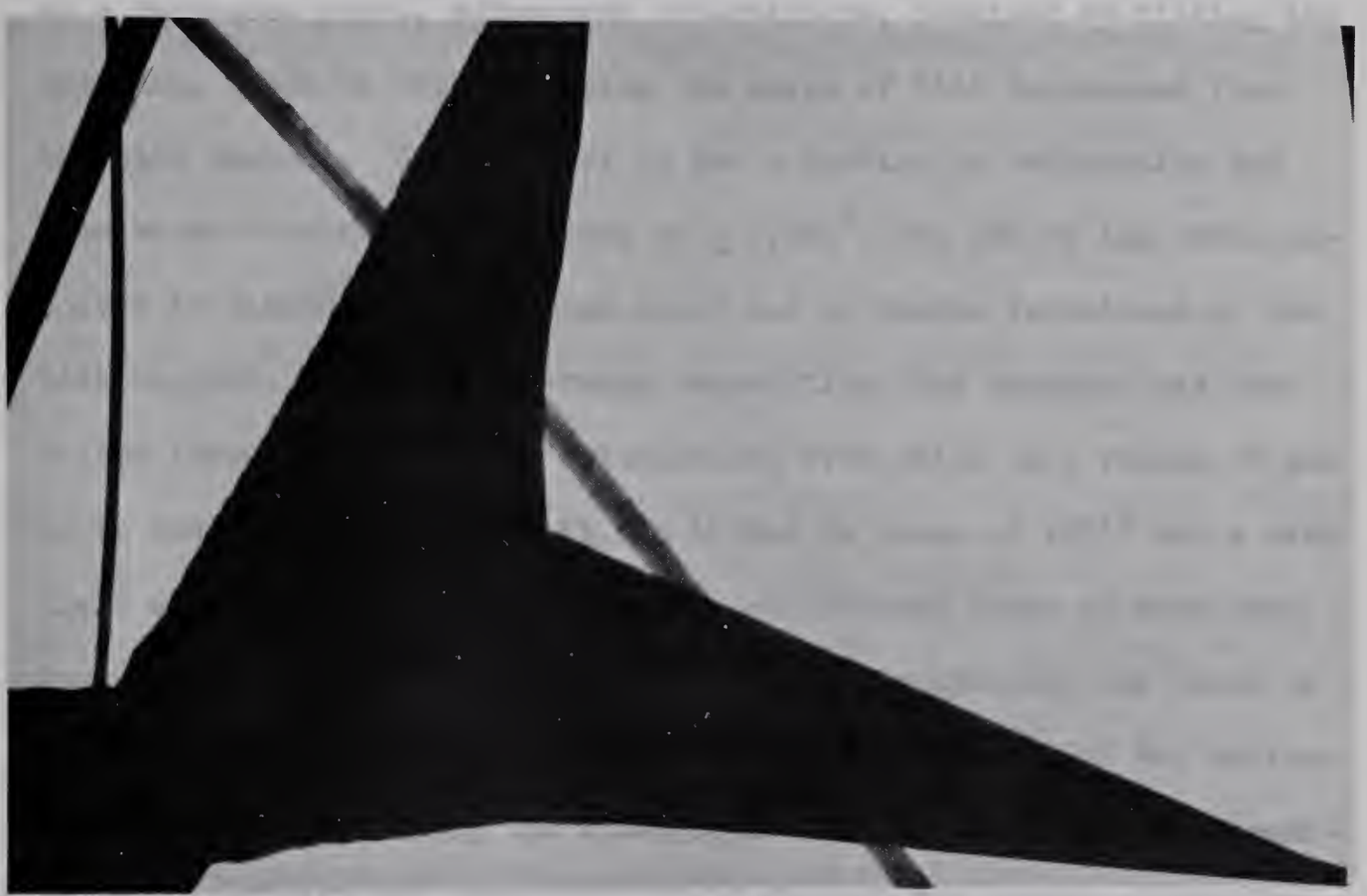

The variation of ξ/ξ_0 with $\Delta\theta$ was found from micrographs obtained in the following manner. After a suitable region of specimen had been found and oriented as described above, it was tilted until one of the higher order systematic reflections was in the Bragg condition, as determined from the Kikuchi pattern. Using this orientation as a reference point, subsequent orientations, obtained by tilting the specimen, could be found by using the angle of tilt determined from the tilt control. The value of $\Delta\theta$ for a particular orientation was then known to within an accuracy of $\pm$ 0.025°, the sum of the errors involved in finding the reference point and in random variations of the tilt control. From the reference orientation, the specimen was then tilted through the range of orientations over which ξ/ξ_0 versus $\Delta\theta$ was to be found. In this range it was tilted in steps of .025° and a dark field micrograph using the reflection of interest taken at each step. In order to be able to find ξ/ξ_0 from these micrographs, the range of tilt was always chosen to include the Bragg orientation of the reflection of interest. Also, the micrographs were taken at constant magnification and with the condenser lens defocused for better resolution. The range of values of $\Delta\theta$ over which these micrographs were taken was approximately twice the Bragg angle of the reflection of interest centered at the Bragg condition for that reflection. For each series of micrographs, a set of diffraction patterns through the same range of orientations were recorded in order to determine the presence of any low-order strongly diffracted beams other than those in the row under

consideration.

(ii) Measurements of ξ_o

These measurements require that the wedge angle of the crystal under study be known. Wagner et al.[25] have studied the morphology of the silicon whiskers produced by the disproportionation method outlined above. They found that the regular whiskers were hexagonal in cross section and had their long axis in a [111] direction. For whiskers whose diameters were less than a micron, the lateral faces were {110} planes. For larger whiskers, however, the lateral faces were usually {211} planes. The morphology of the regular whiskers grown here was checked by comparing micrographs of whiskers with their corresponding electron diffraction patterns. The variation in thickness across the whiskers as determined from the micrographs was correlated with the diffraction patterns to find the planes forming the lateral faces. The results of these measurements for submicron size whiskers were in agreement with those of Wagner et al.[25].

In making the ξ_o measurements, regular whiskers whose orientation and dark field image were similar to that shown in Figure 7 were used. Because of the large wedge angle involved, it was necessary to use only whiskers near a (110) orientation in order to keep rotations of the whisker about its long axis to a minimum. At least three extinction contours were required in the image of a wedge-shaped

Figure 7

Configuration of whisker and image in $\mathcal{E}_o$ measurements.
(a) Perspective drawing of a regular whisker with an electron beam striking its top surface, a (110) plane, at close to a perpendicular angle.
(b) A drawing of the image of the whisker showing the presence of extinction contours resulting from the wedge-shaped regions

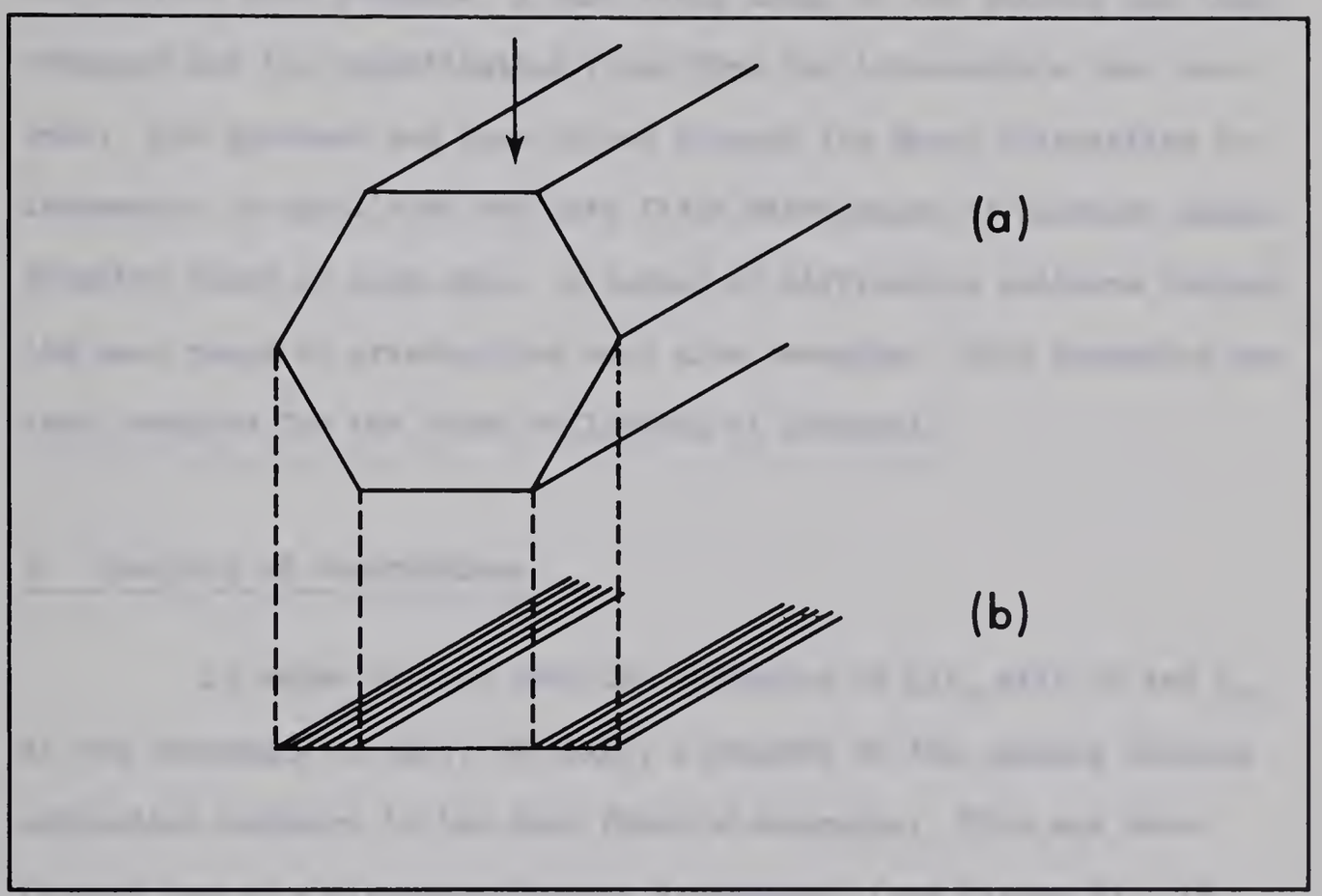

FIGURE 7

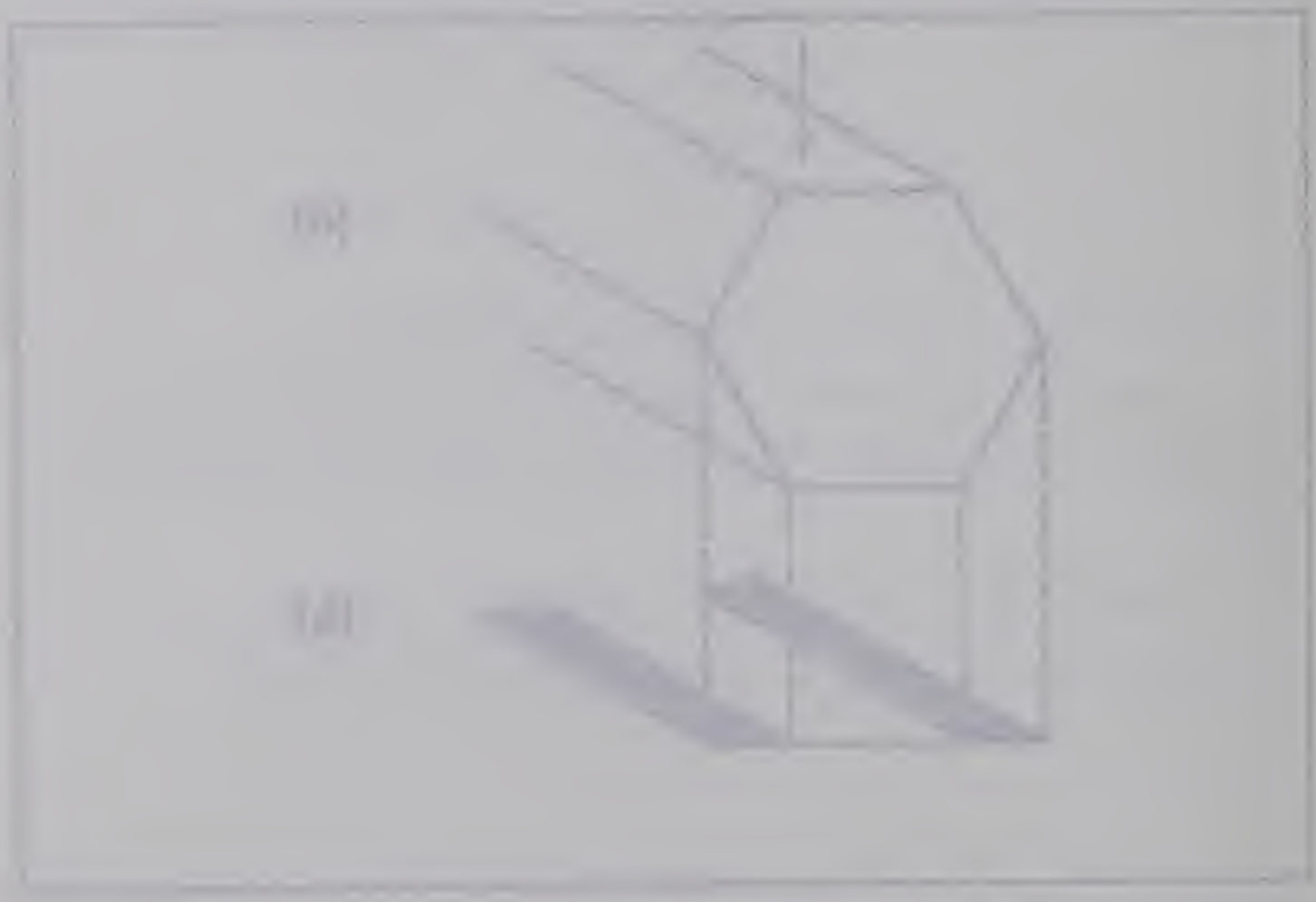

region for accuracy in measuring the spacing.

After a suitable whisker was found, it was oriented so that one of the (111) or (220) reflections present in a (110) diffraction pattern was near its Bragg condition, but no other intense low-order reflections were present. A dark field image of the whisker was then obtained and its magnification found from the intermediate lens current. The specimen was then tilted through the Bragg orientation in increments of equal size and dark field micrographs of constant magnification taken at each step. A series of diffraction patterns through the same range of orientations were also recorded. This procedure was then repeated for the other reflection of interest.

D. Analysis of Observations

In order to find both the variation of $\varepsilon/\varepsilon_o$ with $\Delta\theta$ and ε_o, it was necessary to have, at least, a measure of the spacing between extinction contours in the dark field micrographs. This was done through use of a microdensitometer arrangement (see Figure 8). In this system the micrographs were carried at constant speed through a light beam and the variations in transmitted intensity converted into peaks on a chart recorder (see Figure 9). The spacing was then found by measuring the distance between the peaks. However, before a set of traces were taken, the micrographs were examined for areas where the contours were evenly spaced and where there was no evidence of strains.

Figure 8

Microdensitometer system for measuring the distance between extinction contours

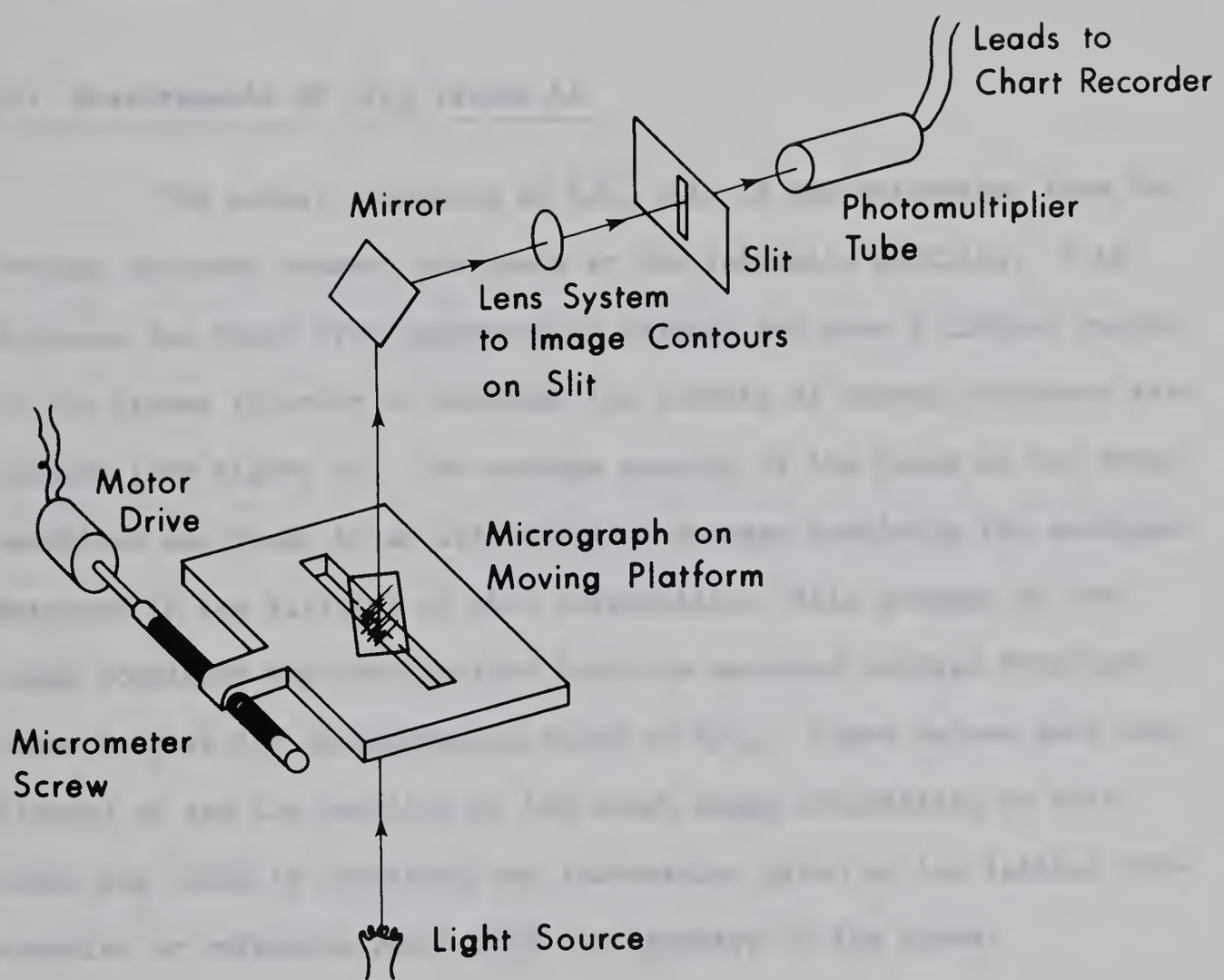
Leads to
Chart Recorder
Photomultiplier
Tube
Slit
Mirror
Lens System
to Image Contours
on Slit
Motor
Drive
Micrograph on
Moving Platform
Micrometer
Screw
Light Source

FIGURE 8

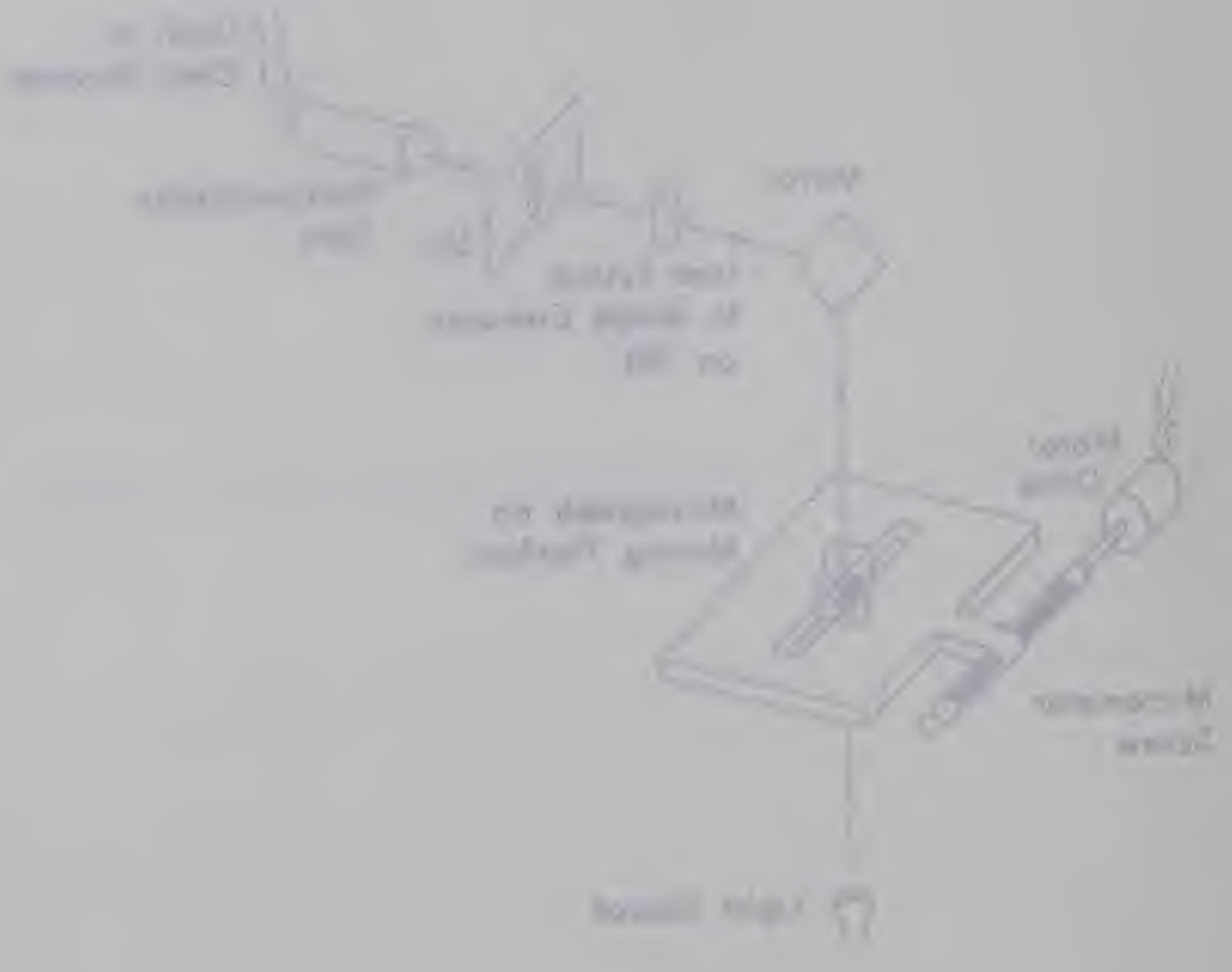

The position of such an area was marked on all the micrographs in the set. These micrographs were then placed in the microdensitometer so that the contours were perpendicular to the direction of travel and traces taken of the marked areas.

(i) Measurements of ξ/ξ_o Versus $\Delta\theta$

The actual variation of ξ/ξ_o with $\Delta\theta$ was determined from the average distance between the peaks in the intensity profiles. This distance was found from measurements carried out over a limited region of the traces in order to minimize the effects of uneven thickness variations (see Figure 9). The average spacing of the peaks at the Bragg condition was found by an interpolation process involving the averages measured in the vicinity of this orientation. This average at the Bragg condition was then divided into the measured average from each trace to give its corresponding value of ξ/ξ_o. These values were then plotted up and the position of the exact Bragg orientation on this curve was found by combining the information given by the initial orientation or reference point with the symmetry of the curve.

(ii) Measurements of ξ_o

In the ξ/ξ_o measurements, it was not necessary to know the actual distance between the contours on the micrographs. However, in measurements of ξ_o this spacing had to be found. This was done from

Figure 9

Microdensitometer traces showing the spacing of the extinction contours

(a) near the Bragg condition.

(b) at a $\Delta\theta$ of 0.275°.

Measurements of the average peak to peak distance would be carried out in the region A to B on all traces corresponding to this set of micrographs

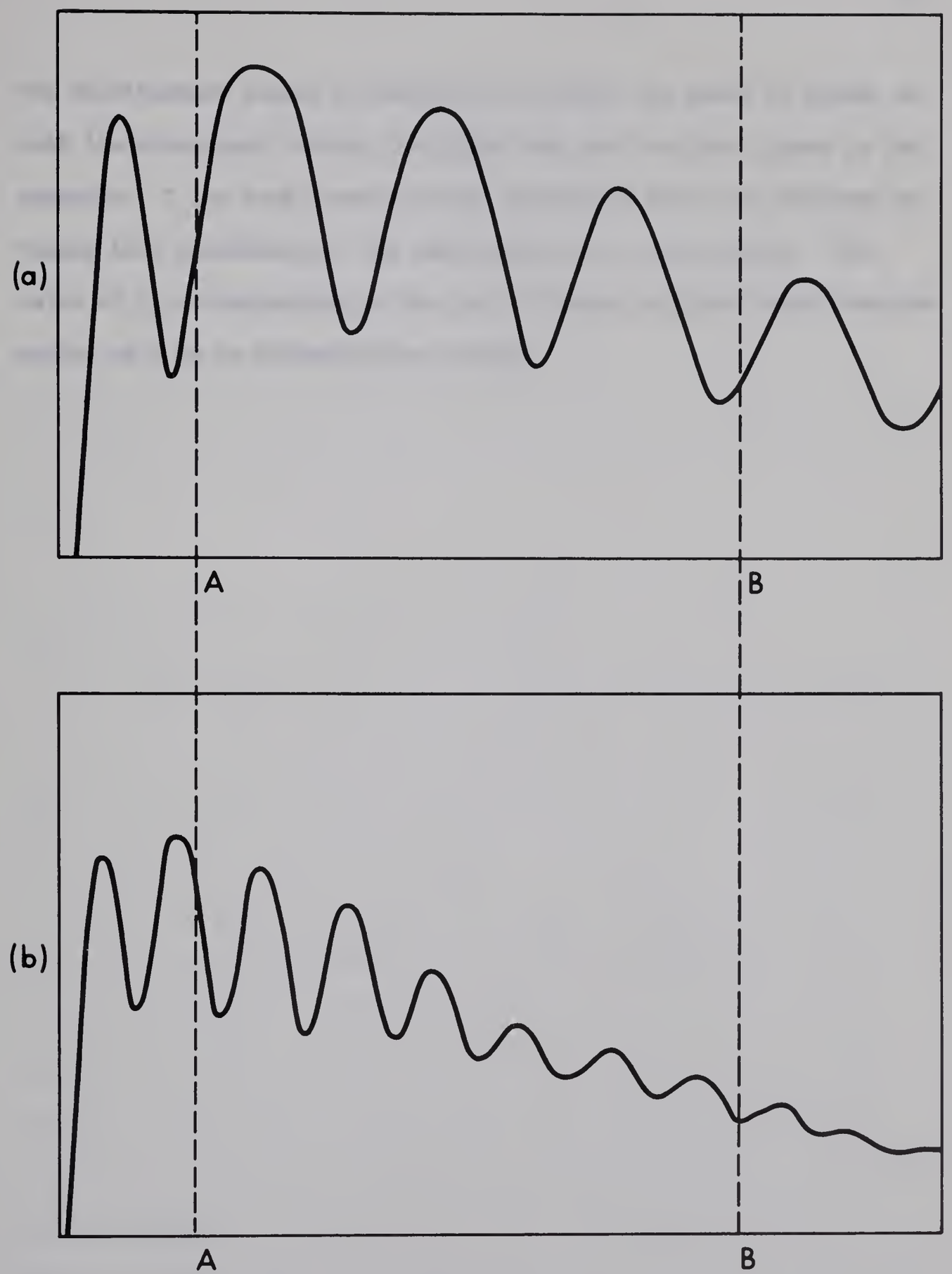

FIGURE 9

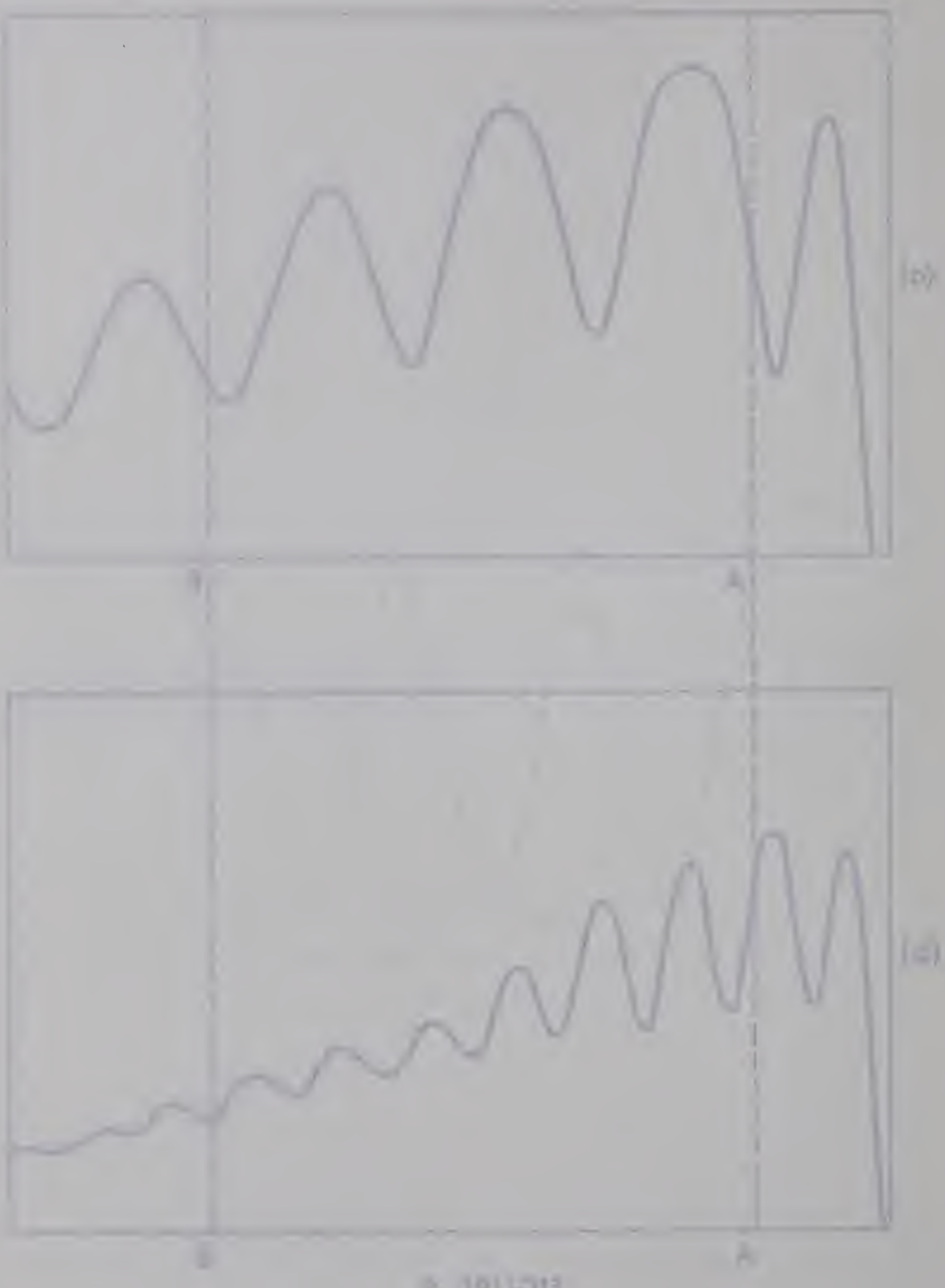
(b)
B
A
(c)
B
A

the densitometer traces by taking into account the rates of travel of both the micrograph through the light beam and the chart paper in the recorder. ξ for each trace was then calculated from this distance by taking into consideration the wedge angle and magnification. The value of ξ_o corresponding to the set of traces was then found from the values of ξ by an interpolation process.

CHAPTER IV

RESULTS

The extinction distance measurements were carried out a number of times for each reflection at each accelerating voltage. The predictions of the two-beam and multi-beam dynamical theories of electron diffraction were then compared with the averages of these measurements.

A. Results of ξ/ξ_o Versus $\Delta\theta$ Measurements

The results of these measurements are presented in Figures 10, 11, 12 and 13 along with the corresponding predictions of the two-beam and multi-beam theories. The experimental results presented in these Figures are the averages of 3, 2, 4 and 5 sets of measurements respectively. Only those results were used in which the variation of ξ/ξ_o with $\Delta\theta$ was relatively smooth, showing no recognizable effects resulting from non-systematic reflections. These effects could be detected by the sharp changes which occurred in the ξ/ξ_o versus $\Delta\theta$ curves (see Figure 14). These changes were found to be associated with a non-systematic reflection near its Bragg condition. The experimental averages are given in the Figures 10 to 13 with a range of error of $\pm 2\frac{1}{2}$ per cent. The experimental results all fell within this

Figure 10

The variation of ξ/ξ_o with $\Delta\theta$ for the (220) reflection in silicon at 100 kV

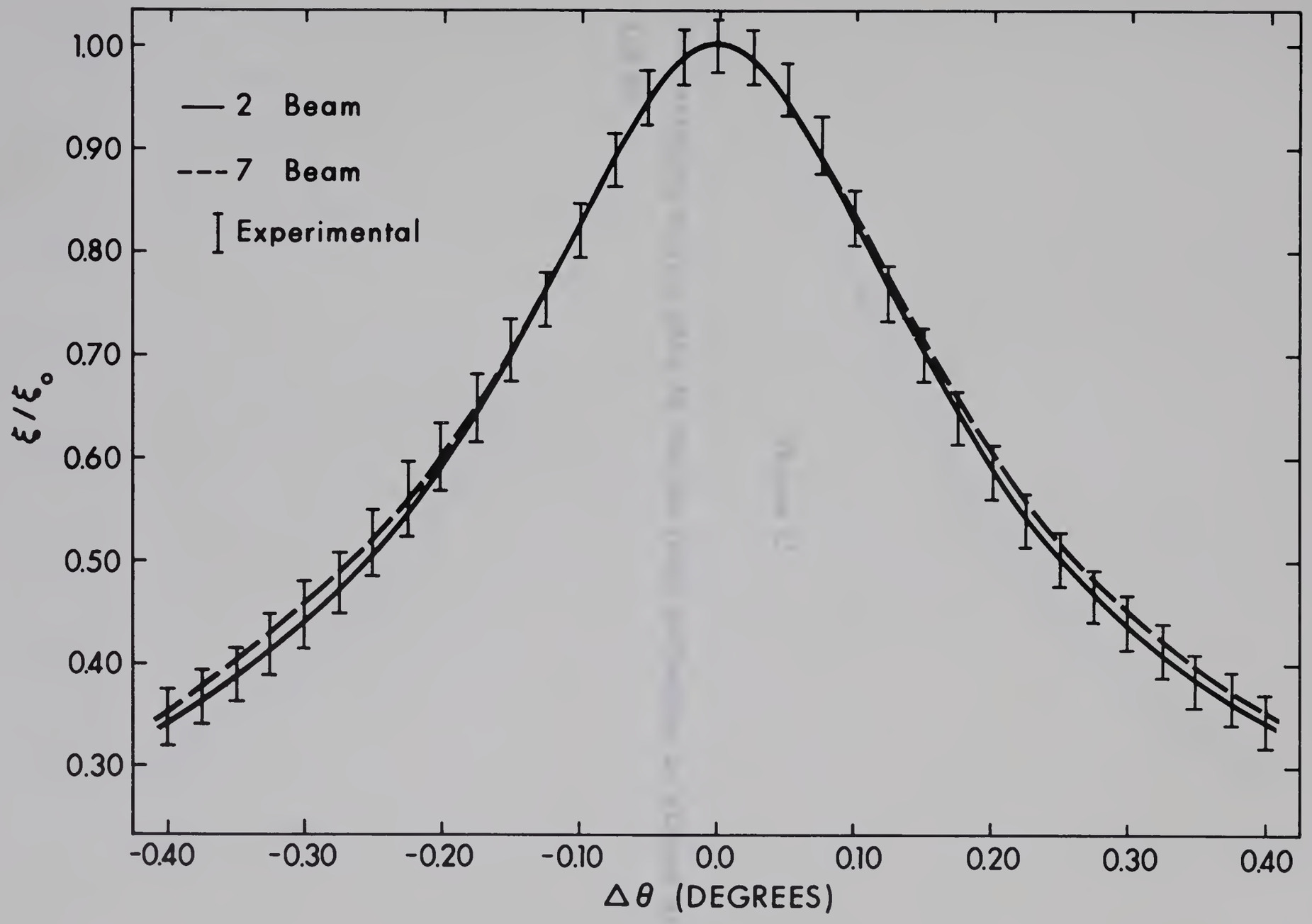
1.00
0.90
0.80
0.70
0.60
0.50
0.40
0.30
ξ/ξ₀
2 Beam
7 Beam
Experimental
-0.40
-0.30
-0.20
-0.10
0.0
0.10
0.20
0.30
0.40
Δθ (DEGREES)

FIGURE 10

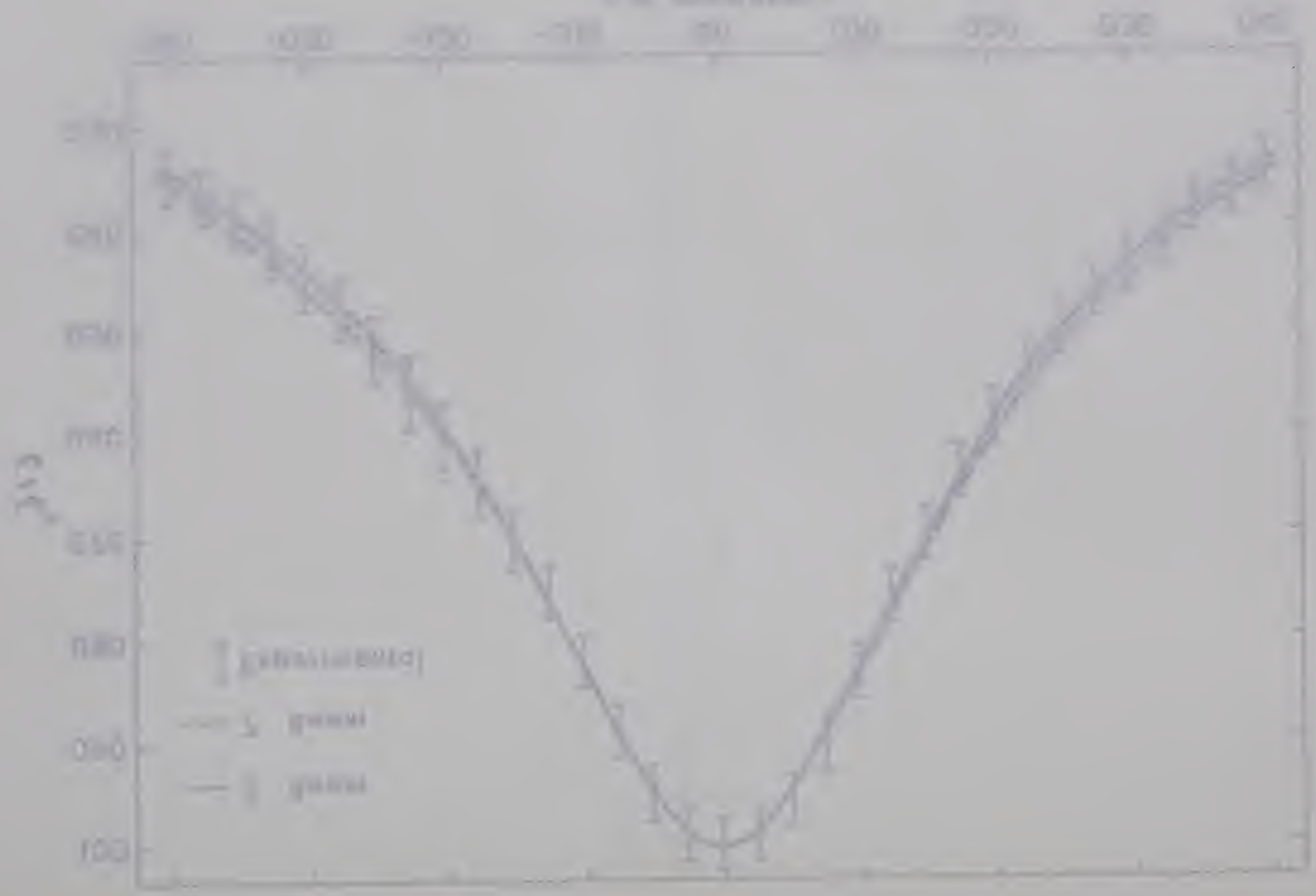

Figure 11

The variation of ξ/ξ_0 with $\Delta\theta$ for the (220) reflection in silicon at 152 kV

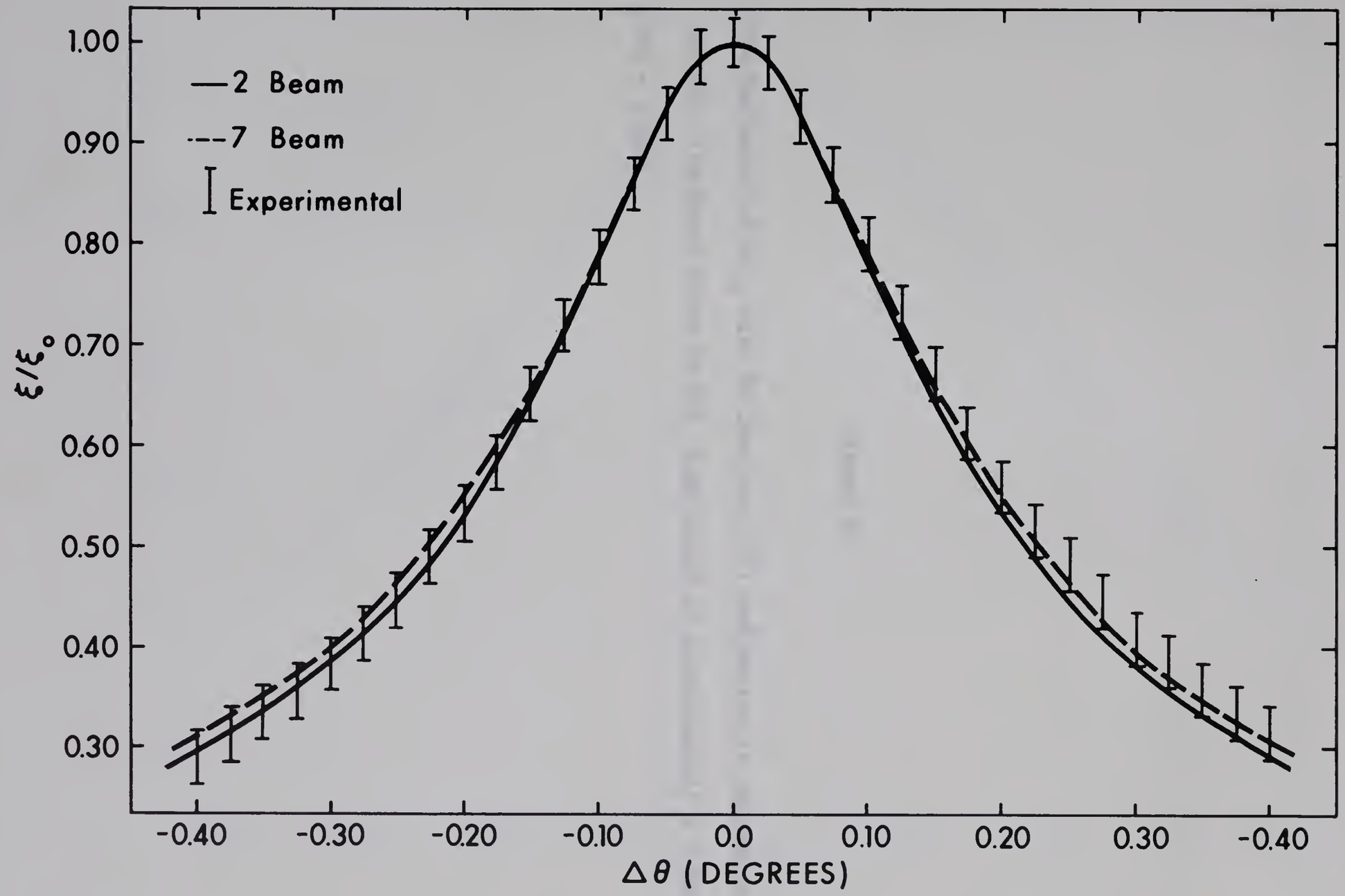
1.00
0.90
0.80
0.70
0.60
0.50
0.40
0.30
ξ/ξ₀
—2 Beam
---7 Beam
Experimental
-0.40
-0.30
-0.20
-0.10
0.0
0.10
0.20
0.30
-0.40
Δθ (DEGREES)

FIGURE 11

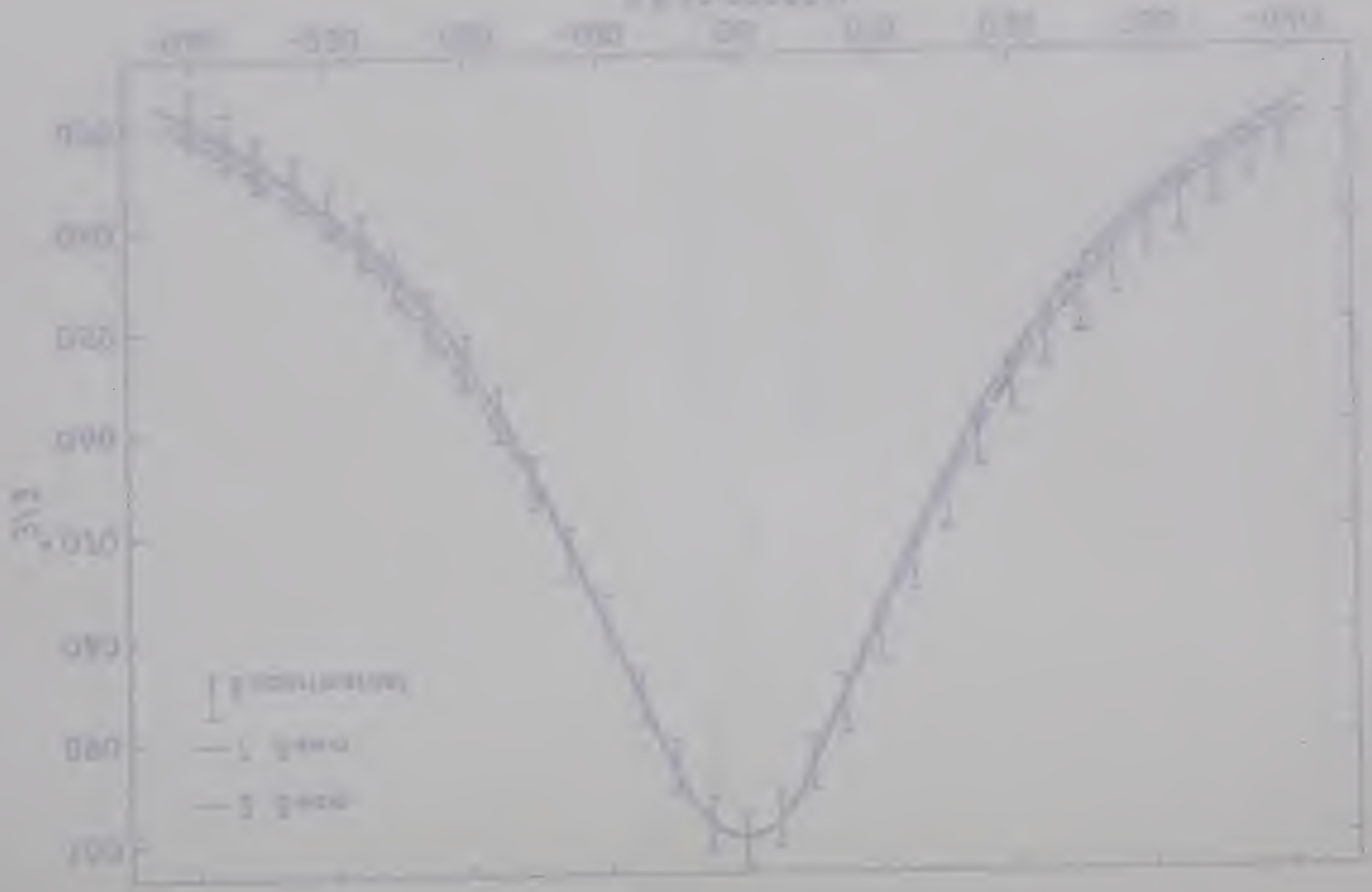

Figure 12

The variation of $\mathcal{E}/\mathcal{E}_o$ with $\Delta\theta$ for the (111) reflection in silicon at 100 kV. The sharp drops in $\mathcal{E}/\mathcal{E}_o$ take place at approximately + 0.260° and - 0.300°

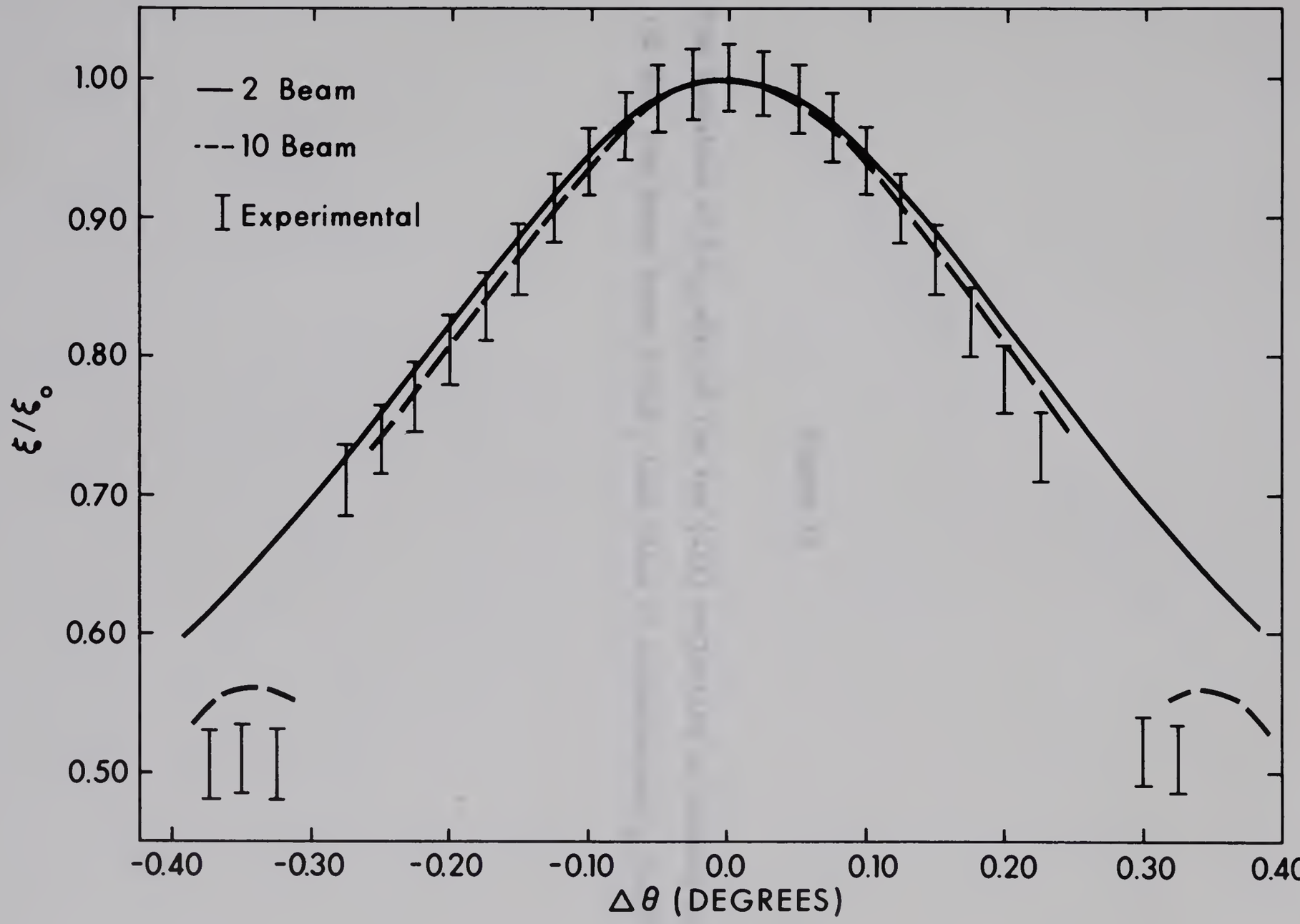
1.00
0.90
0.80
0.70
0.60
0.50
ξ/ξ₀
— 2 Beam
--- 10 Beam
I Experimental
-0.40
-0.30
-0.20
-0.10
0.0
0.10
0.20
0.30
0.40
Δθ (DEGREES)

FIGURE 12

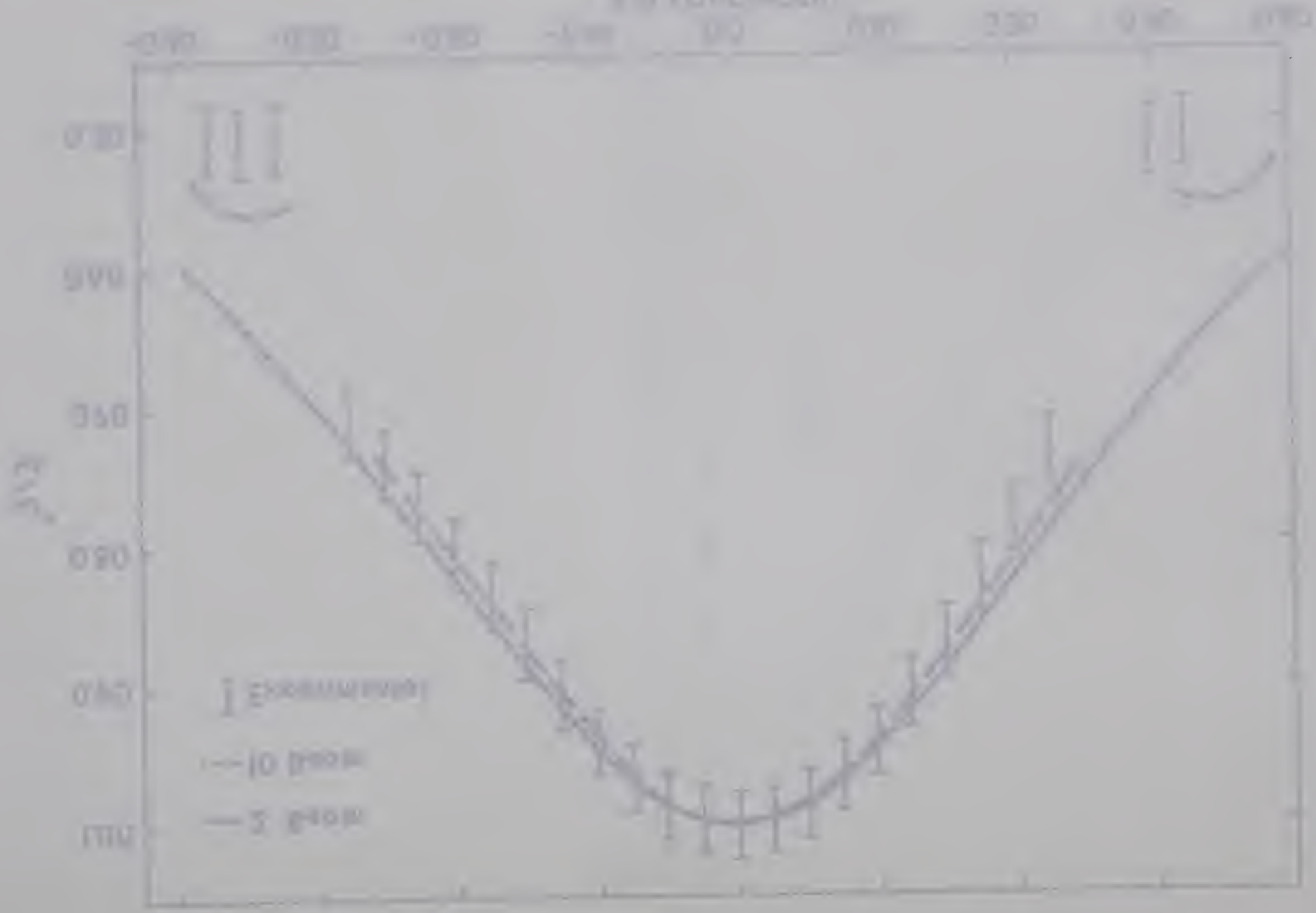

Figure 13

The variation of ξ/ξ_o with $\Delta\theta$ for the (111) reflection in silicon at 152 kV. The sharp drops in ξ/ξ_o take place at approximately $\pm$ 0.210°

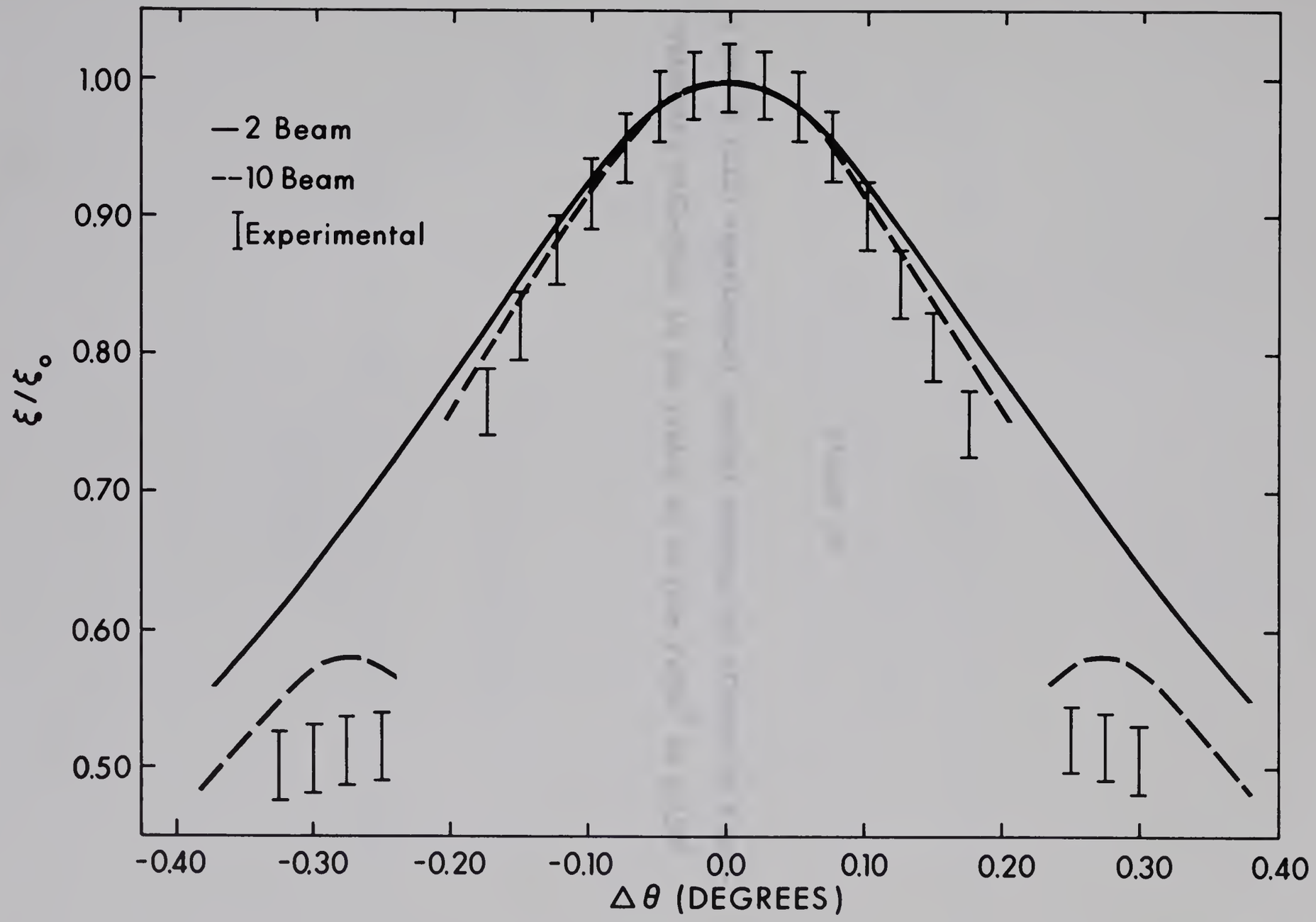
1.00
0.90
0.80
0.70
0.60
0.50
ξ/ξ₀
—2 Beam
--10 Beam
Experimental
-0.40
-0.30
-0.20
-0.10
0.0
0.10
0.20
0.30
0.40
Δθ (DEGREES)

FIGURE 13

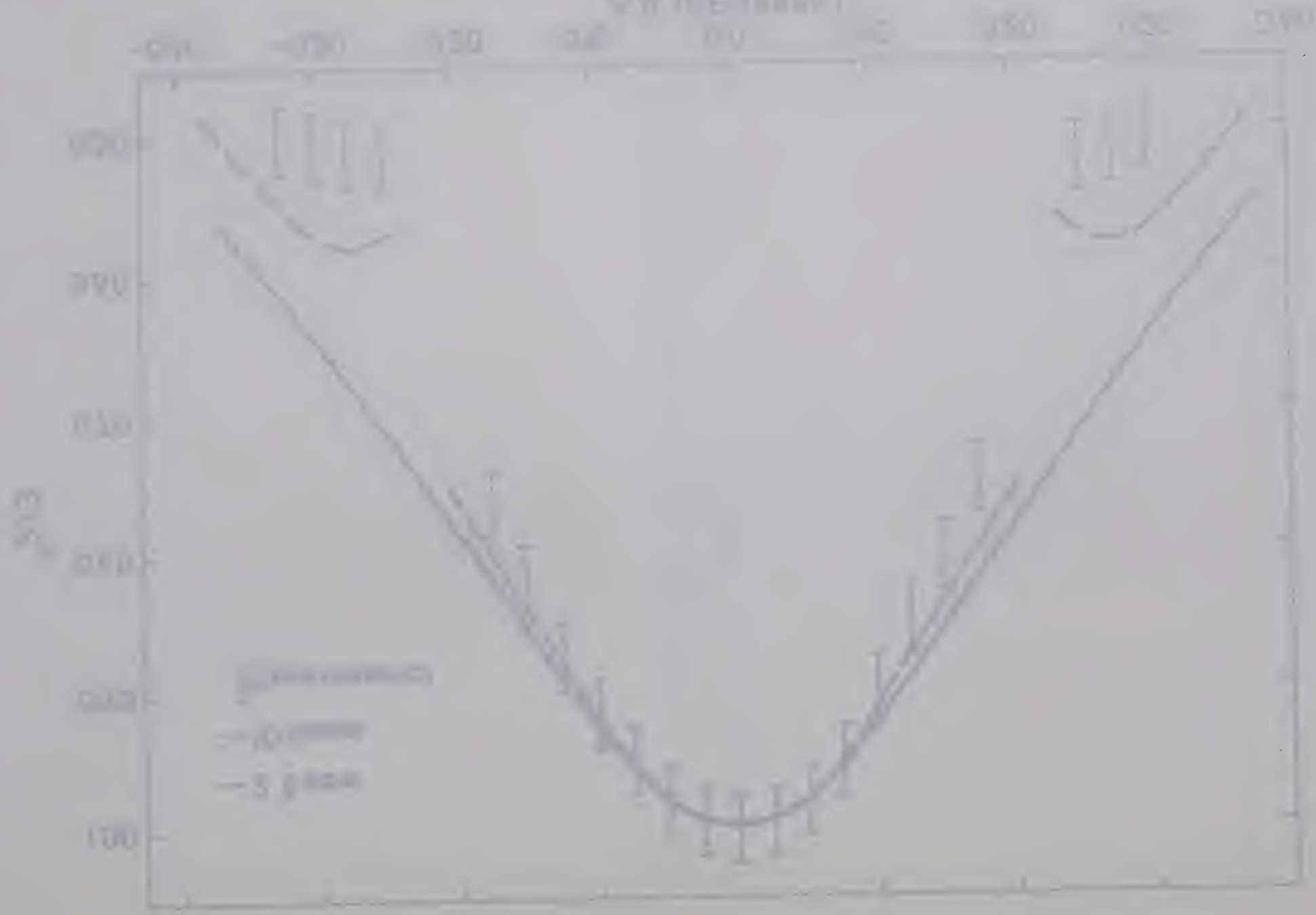

Figure 14

A set of (111) experimental results showing the effects of a non-systematic reflection in the region of $\Delta\theta$ from 0.050° to 0.150°

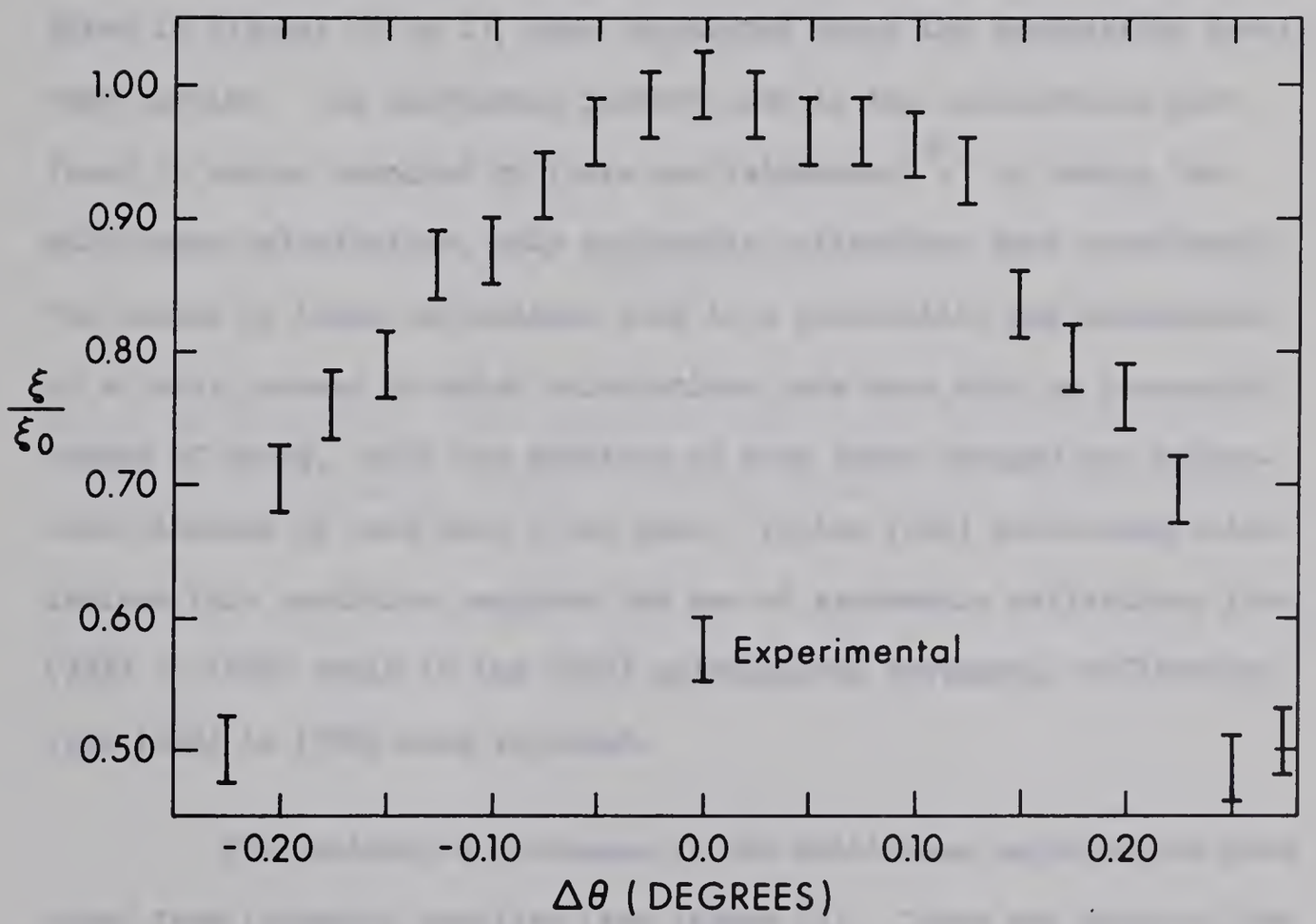
1.00
0.90
0.80
0.70
0.60
0.50
ξ/ξ0
Experimental
-0.20
-0.10
0.0
0.10
0.20
Δθ (DEGREES)

FIGURE 14

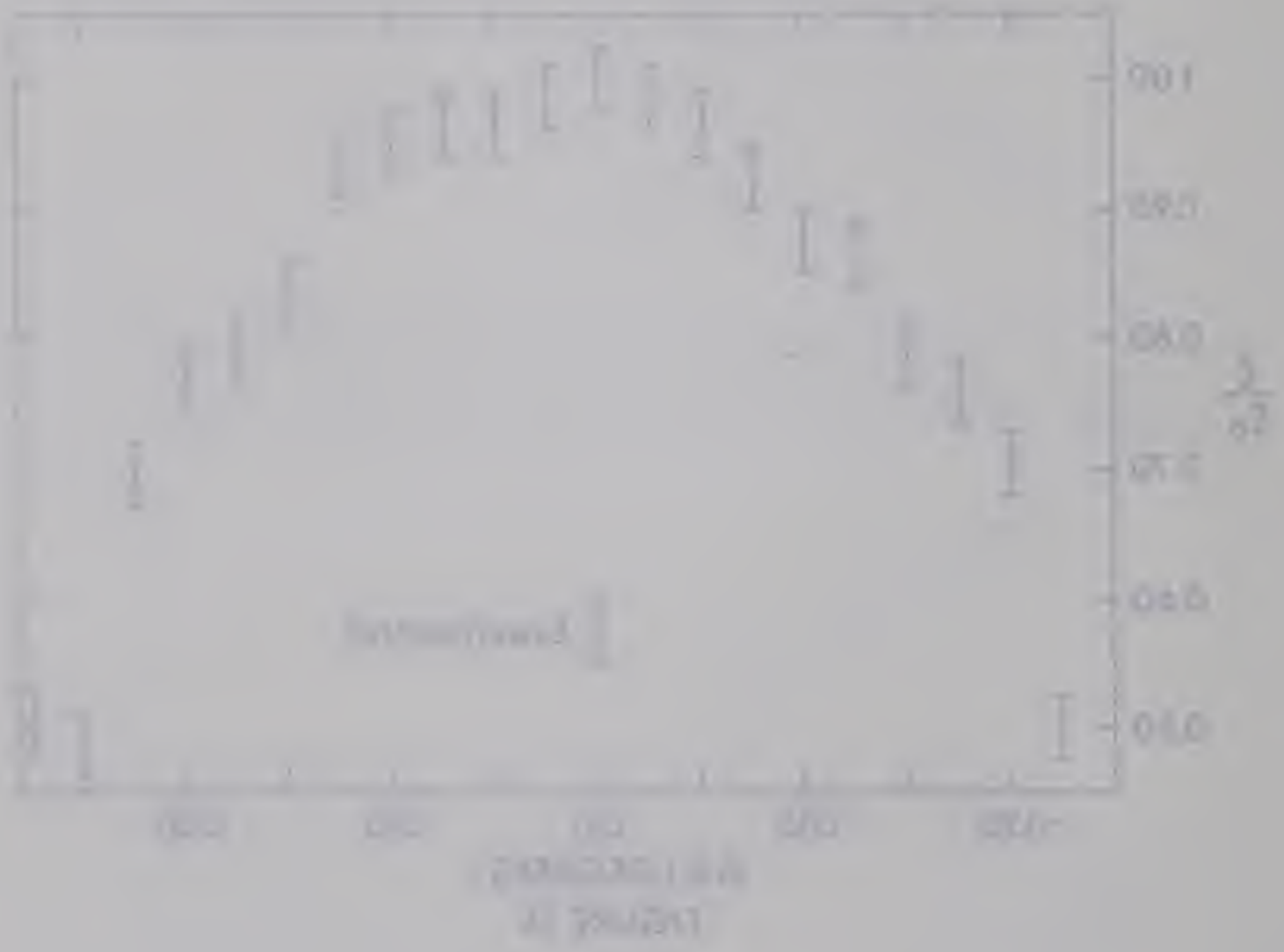

range except where shown by the extended error bars. This range of error of $\pm 2\frac{1}{2}$ per cent arises in the measurement of the distance between peaks in the densitometer traces due to the difficulty in defining the exact position of the peaks.

The predictions of the two-beam and multi-beam theories, given in Figures 10 to 13, were calculated using the expressions developed earlier. The scattering factors used in the calculations were found in tables compiled by Ibers and Vainshtein[28]. In making the multi-beam calculations, only systematic reflections were considered. The number of these reflections used in a calculation was determined by a trial process in which calculations were made with an increasing number of beams, until the addition of more beams changed the extinction distance by less than 1 per cent. In the (111) multi-beam calculations this condition required the use of systematic reflections from $(\bar{3}\bar{3}\bar{3})$ to (666) while in the (220) calculations systematic reflections from $(\bar{4}\bar{4}0)$ to (880) were required.

The extinction distances in the multi-beam calculations were found from intensity profiles (see Figure 15). These are plots of the variation of the intensity of the beam under consideration with depth in the crystal, as obtained from an autoplotter system used in conjunction with a computer. The extinction distance was found by measuring the average distance between the peaks. Attenuation was not taken into consideration in these calculations as preliminary calculations showed

Figure 15

An intensity profile of the variation with depth of the (111) diffracted beam intensity at 152 kV as found from a 10-beam approximation

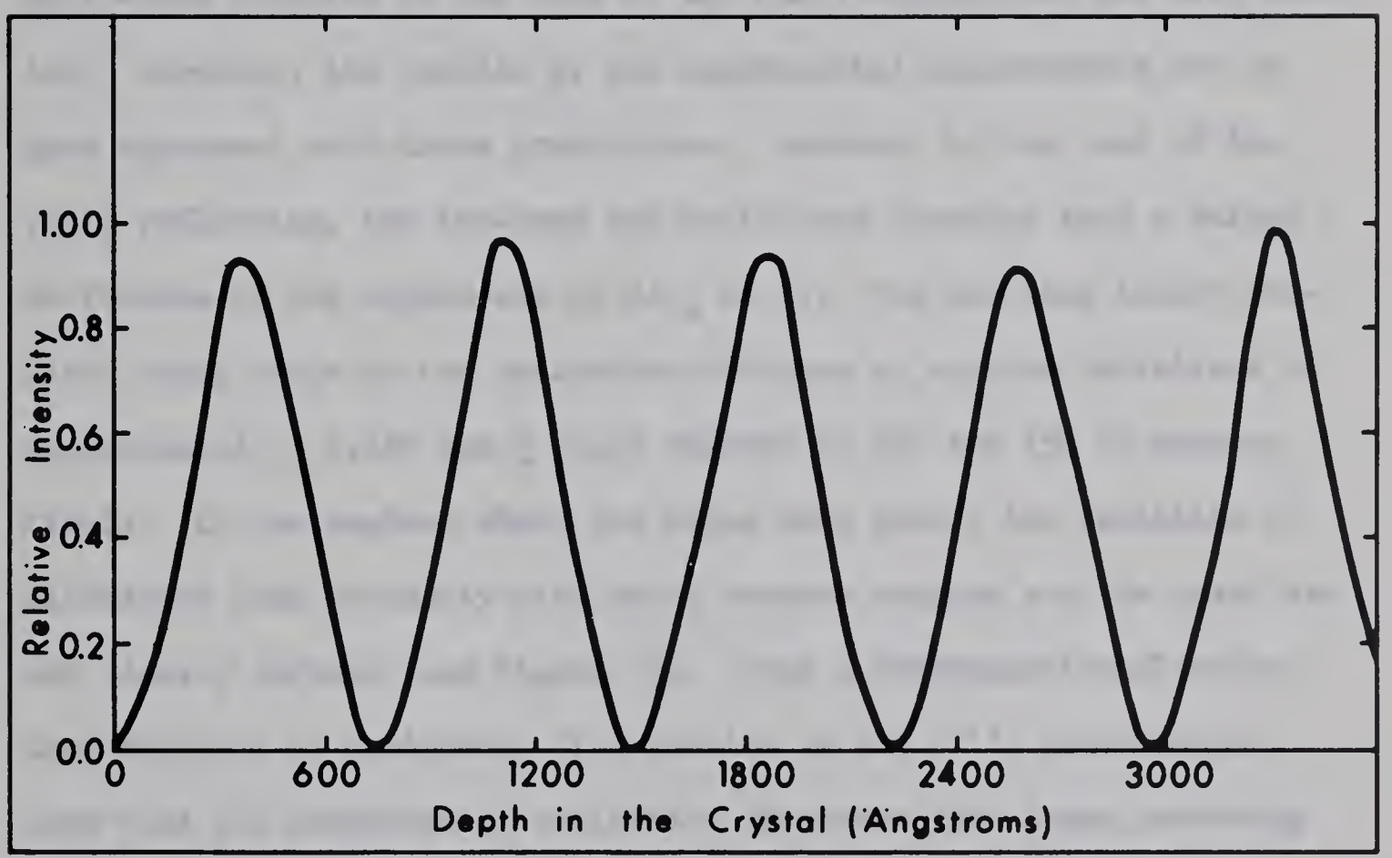
1.00
0.8
0.6
0.4
0.2
0.0
Relative Intensity
0
600
1200
1800
2400
3000
Depth in the Crystal (Angstroms)

FIGURE 15

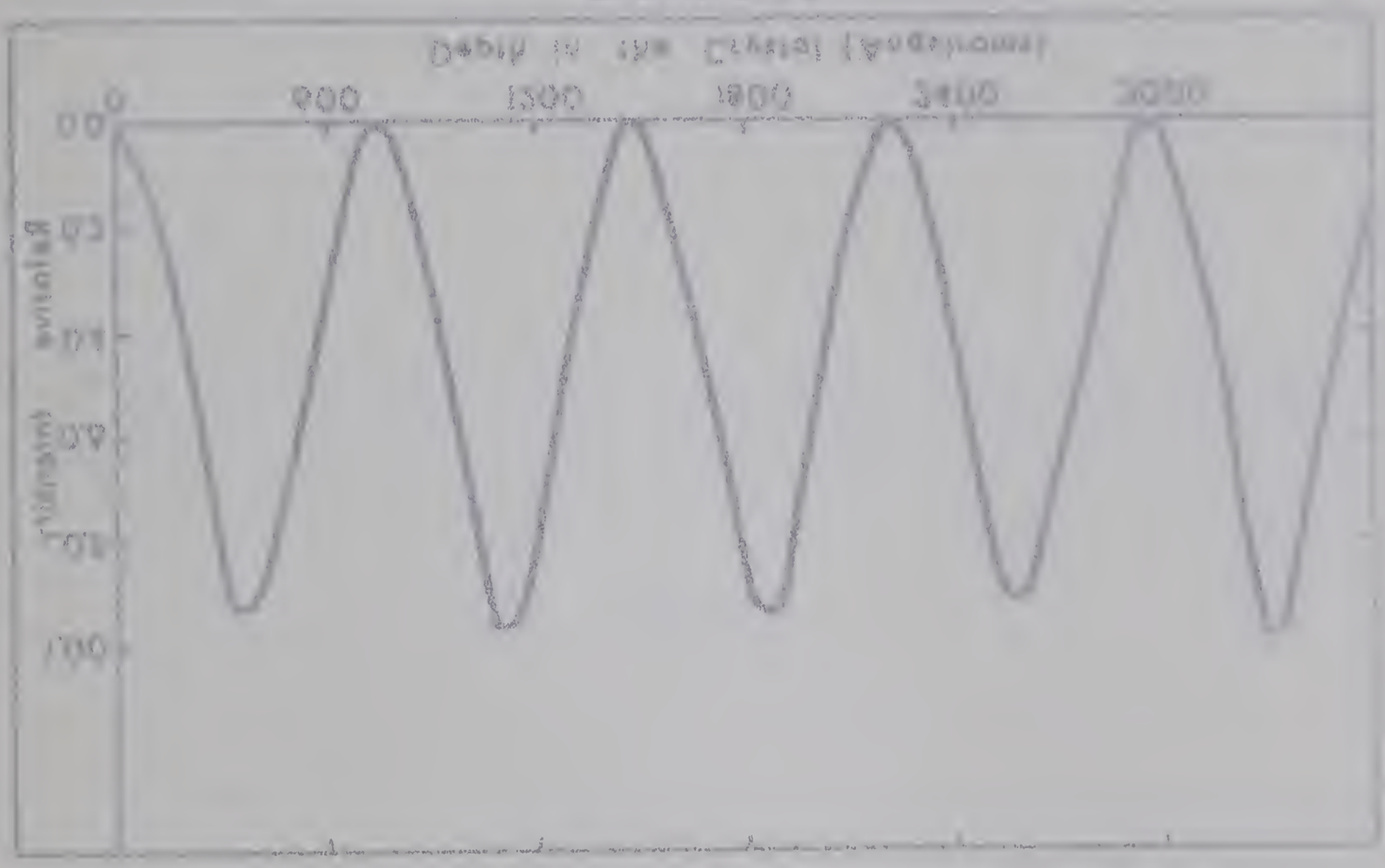

that it would result in less than a 1 per cent correction to the calculated extinction distances.

The actual effect of the systematic reflections on the extinction distance is different for the (220) and (111) reflections. As can be seen in Figures 10 and 11, the predictions of the two-beam and multi-beam theories in the case of the (220) reflections are very similar. Moreover, the results of the experimental measurements are in good agreement with these predictions. However, in the case of the (111) reflection, the two-beam and multi-beam theories show a marked difference in the dependence of ξ/ξ_o on $\Delta\theta$. The two-beam theory predicts sharp drops in the extinction distance at angular deviations of approximately $\pm$ 0.280 and $\pm$ 0.225 degrees at 100 and 152 kV respectively. In the regions where the drops take place, the variation of diffracted beam intensity with depth becomes complex and the peaks are not clearly defined (see Figure 16). Thus a determination of extinction distance is ambiguous. The results of the (111) measurements show that the experimental extinction distances have drops, occurring in the same general range of $\Delta\theta$'s, which are similar to the ones predicted by the multi-beam theory. Moreover, in the regions where the drops occur, the intensity variation becomes complex (see Figure 17). However, the experimental extinction distances at both 100 and 152 kV decrease more rapidly than either the two-beam or multi-beam theories predict. The results at 100 kV show some asymmetry with respect to

Figure 16

Complex depth periodicity of the (111) reflection at 152 kV as predicted by the 10-beam approximation for $\Delta\theta = 0.250$

Figure 17

A densitometer trace of the extinction contours corresponding to the (111) reflection at 152 kV showing the complex periodicity at $\Delta\theta = 0.200^{\circ}$

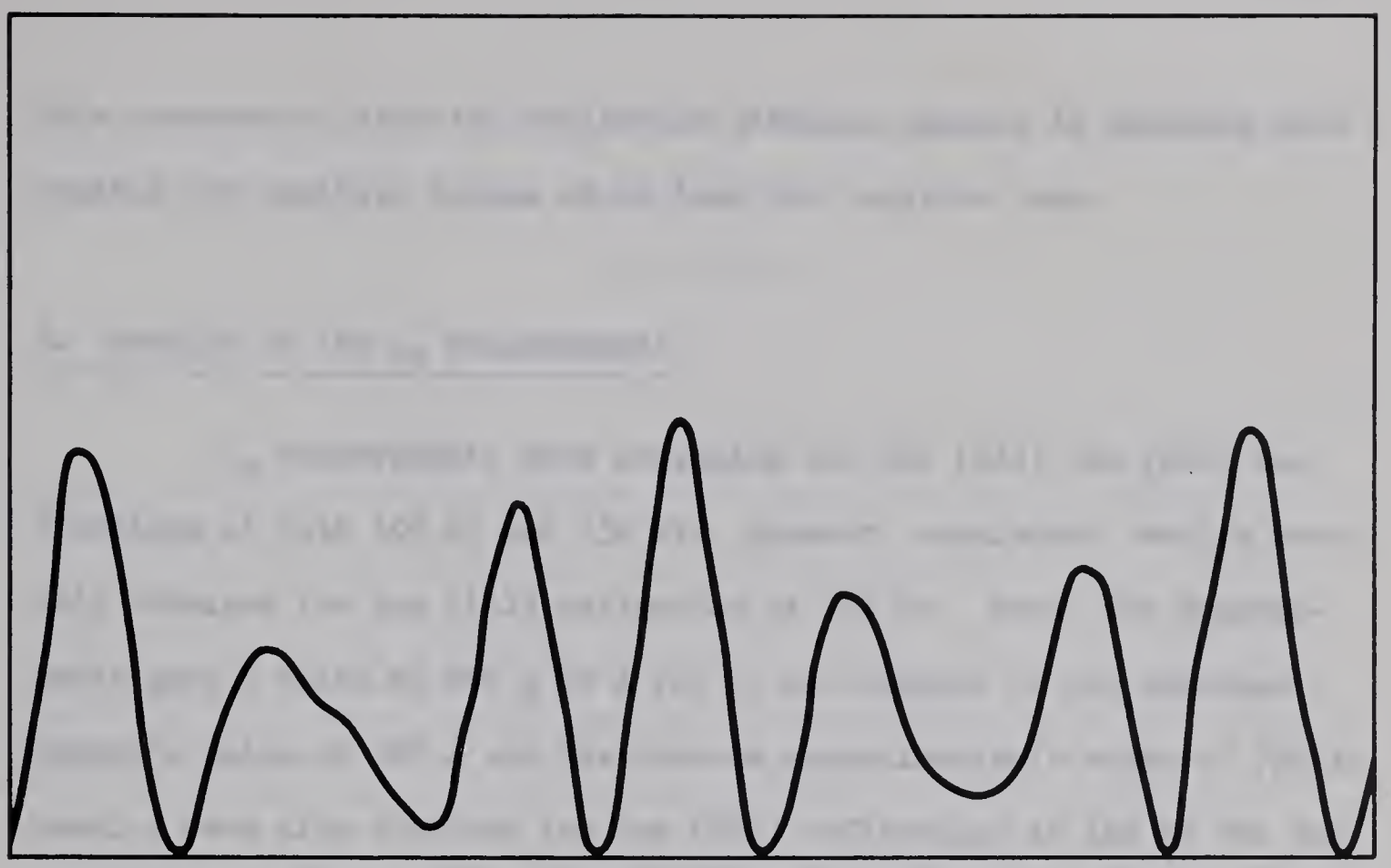

FIGURE 16

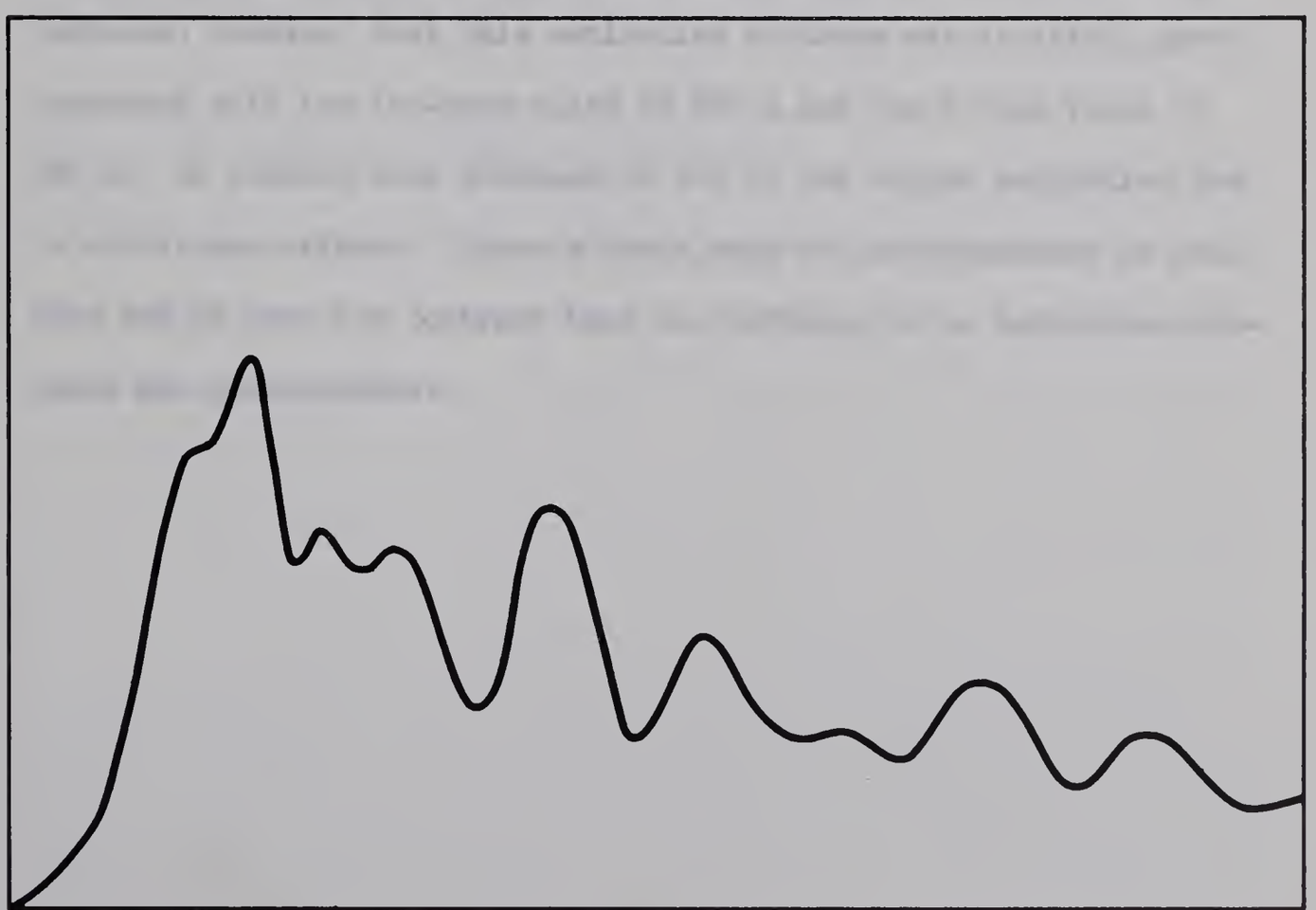

FIGURE 17

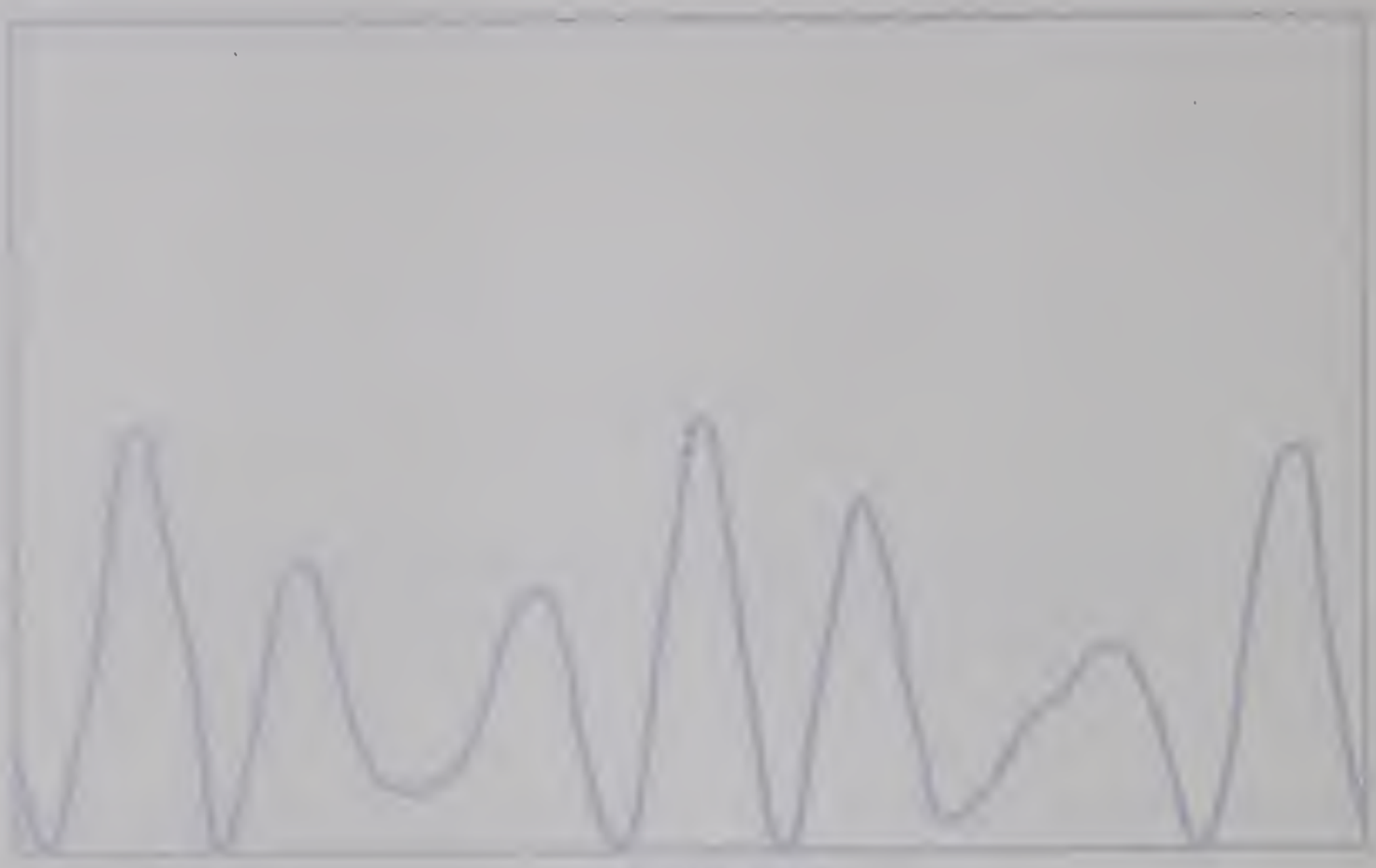

FIGURE 16

FIGURE 17

this decrease in that the extinction distance appears to decrease more rapidly for positive values of $\Delta\theta$ than for negative ones.

B. Results of the ξ_o Measurements

ξ_o measurements were attempted for the (111) and (220) reflections at both 100 kV and 152 kV. However, consistent results were only obtained for the (111) reflection at 152 kV. Here, the measurements gave a value of 840 $\pm$ 40 A for ξ_o as compared to the two-beam theory's value of 720 A and the 10-beam approximation's value of 736 A. Results were also obtained for the (220) reflections at 152 kV but due to multi-beam effects the scatter was quite large. The results did indicate, however, that this extinction distance was in fairly good agreement with the two-beam value of 880 A and the 7-beam value of 840 A. No results were obtained at 100 kV for either reflection due to multi-beam effects. These effects made the periodicities so complex and of such low contrast that the defining of an extinction distance was questionable.

CHAPTER V

DISCUSSION

The results of the extinction distance measurements indicate both agreement and disagreement with theory, depending on which reflection is being considered. The (111) extinction distance varies with $\Delta\theta$ in a manner different from the predictions of both the two-beam and multi-beam approximations. ξ_o measurements for this reflection also disagree with both approximations. The (220) extinction distance, however, shows good agreement with the two approximations for both ξ/ξ_o versus $\Delta\theta$ and ξ_o.

A. (111) Extinction Distance Measurements

As seen in Figures 12 and 13, the (111) experimental extinction distance showed a sharp decrease similar to that predicted by the 10-beam approximation. However, the size of the drop was greater than that predicted by this theory. Also, the measured value of ξ_o for this reflection was 20 per cent larger than the theory predicted.

A possible explanation of these results lies in the values of the scattering factors[28] used in making the theoretical calculations. Ibers[29] has given a discussion of the calculation of the scattering factors and the sources of error involved. For silicon, the

factors were calculated using Hartree-Fock self-consistent wave functions. In using this type of function, he pointed out that there were two possible sources of error. The first of these were errors, either of omission or of calculation, in the contributions to the atomic fields of the outer electrons. The second were errors arising from the use of Hartree-Fock wave functions, calculated for spherically neutral atoms, for an atom in a crystal lattice. In a later paper[30] he gave the following limits to the accuracies of the scattering factors due to these errors. For values of sin θ/λ greater than 0.3 A^{-1} the factors are reliable to 10 per cent but for sin θ/λ less than 0.1 A^{-1} the error may be as large as 50 to 100 per cent. Here, θ is one half of the scattering angle and λ is the wavelength of the incident electron. In the case of the (111) reflection in silicon sin θ/λ is equal to 0.159 A^{-1}. Thus, the scattering factor for this reflection can only be considered accurate to approximately 30 per cent.

An experimental value for the (111) scattering factor was calculated by varying the value of the (111) scattering factor used in the 10-beam approximation until a value of 840 A was found for ξ_o, the (111) extinction distance at 152 kV. The value of scattering factor found in this way was 2.83 A. This experimental value is within 14 per cent of the value of 3.26 A given by Ibers and Vainshtein. Using this new value of scattering factor for the (111) reflection, the variation of ξ with $\Delta\theta$ was recalculated in the case of the 10-beam

approximation and compared with the experimental results (see Figures 18 and 19). The good agreement between the experimental results and the new empirical curve is especially noticable in Figure 19 which shows the results at 152 kV. As was seen in Figure 13, the experimental results dropped below both the two-beam and 10-beam curves even at angular deviations smaller than that at which the sharp drops took place. However, as seen in Figure 19, the new empirical curve passes through all the experimental points between -0.175 and + 0.175. Moreover, the size of the sharp drop as predicted by the empirical curve gives better agreement than the theoretical curves of Figure 13. Thus, it can be seen that the ξ/ξ_0 versus $\Delta\theta$ measurements confirm an experimental value of the scattering factor of 2.83 A.

At 100 kV the fit between the experimental results and empirical curve is not as good as at 152 kV (see Figures 18 and 19). Here, the asymmetry of the experimental results at 100 kV is again demonstrated as the results at negative $\Delta\theta$, before the drop takes place, fall above the empirical curve, while for the corresponding values of positive $\Delta\theta$, the results fall on the curve. A possible explanation for this asymmetry lies in the effect of non-systematic reflections arising from the orientations of the specimens. In the specimens chosen for this set of ξ/ξ_0 measurements, it was observed that low-order non-systematic reflections approached and passed through their Bragg conditions as the specimens were tilted in the

Figure 18

A comparison of the variation of $\varepsilon/\varepsilon_o$ with $\Delta\theta$ as measured for the (111) reflection at 100 kV with the corresponding predictions of a 10-beam approximation calculated using the experimental value of 2.83 A for the (111) scattering factor

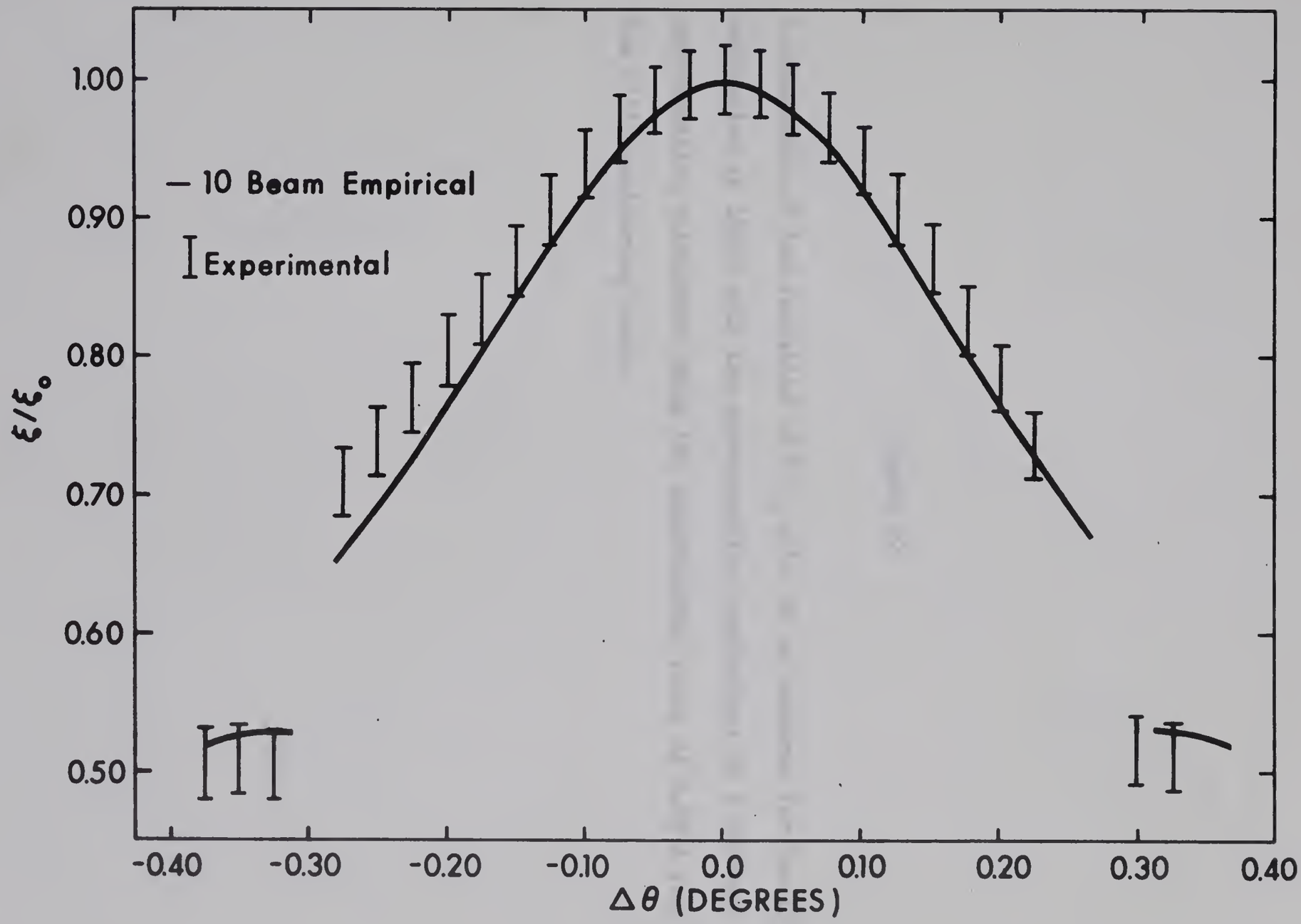
1.00
0.90
0.80
0.70
0.60
0.50
ε/ε₀
— 10 Beam Empirical
Experimental
-0.40
-0.30
-0.20
-0.10
0.0
0.10
0.20
0.30
0.40
Δθ (DEGREES)

FIGURE 18

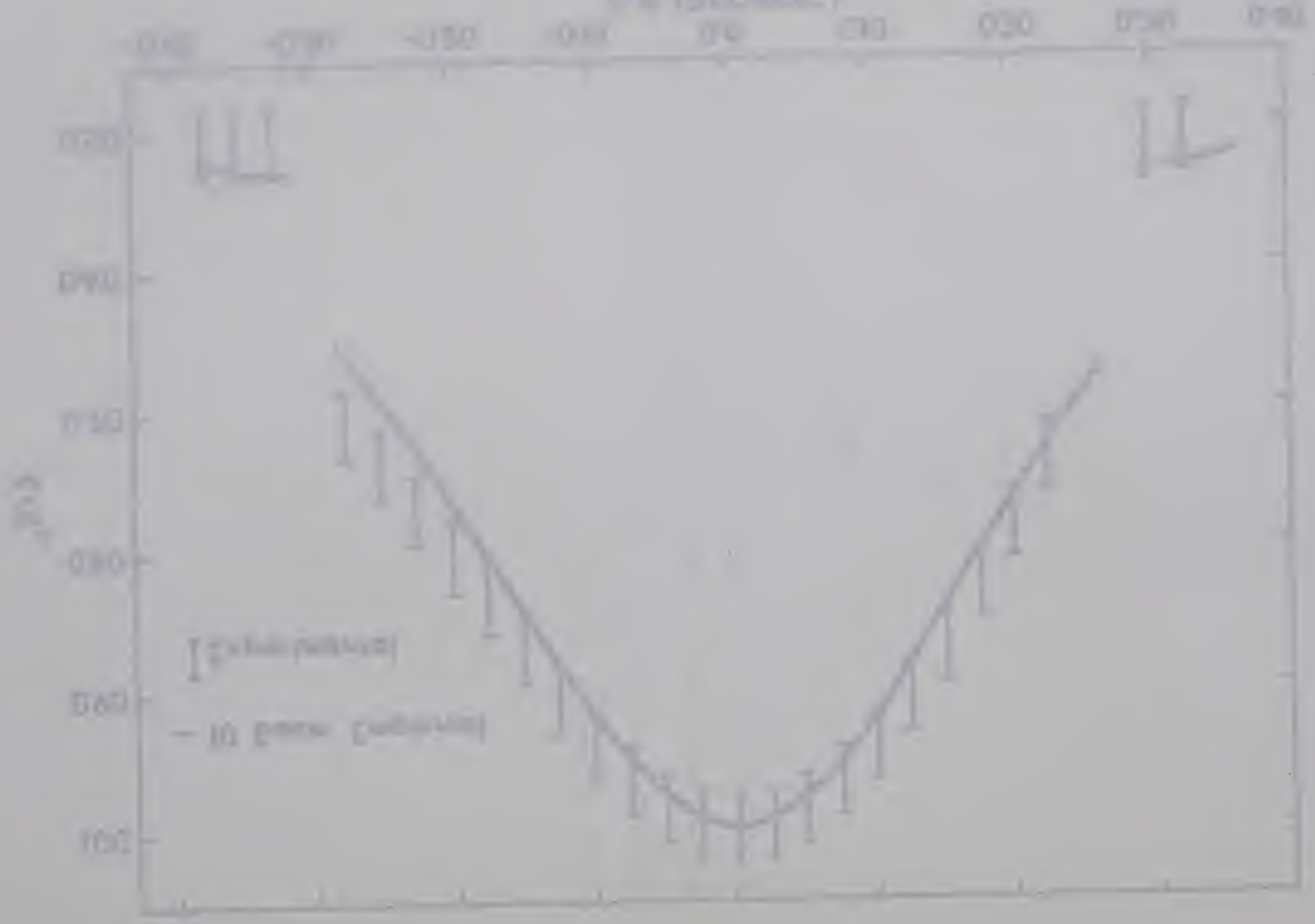

Figure 19

A comparison of the variation of ξ/ξ_o with $\Delta\theta$ as measured for the (111) reflection at 152kV with the corresponding predictions of a 10-beam approximation calculated using the experimental value of 2.83 A for the (111) scattering factor

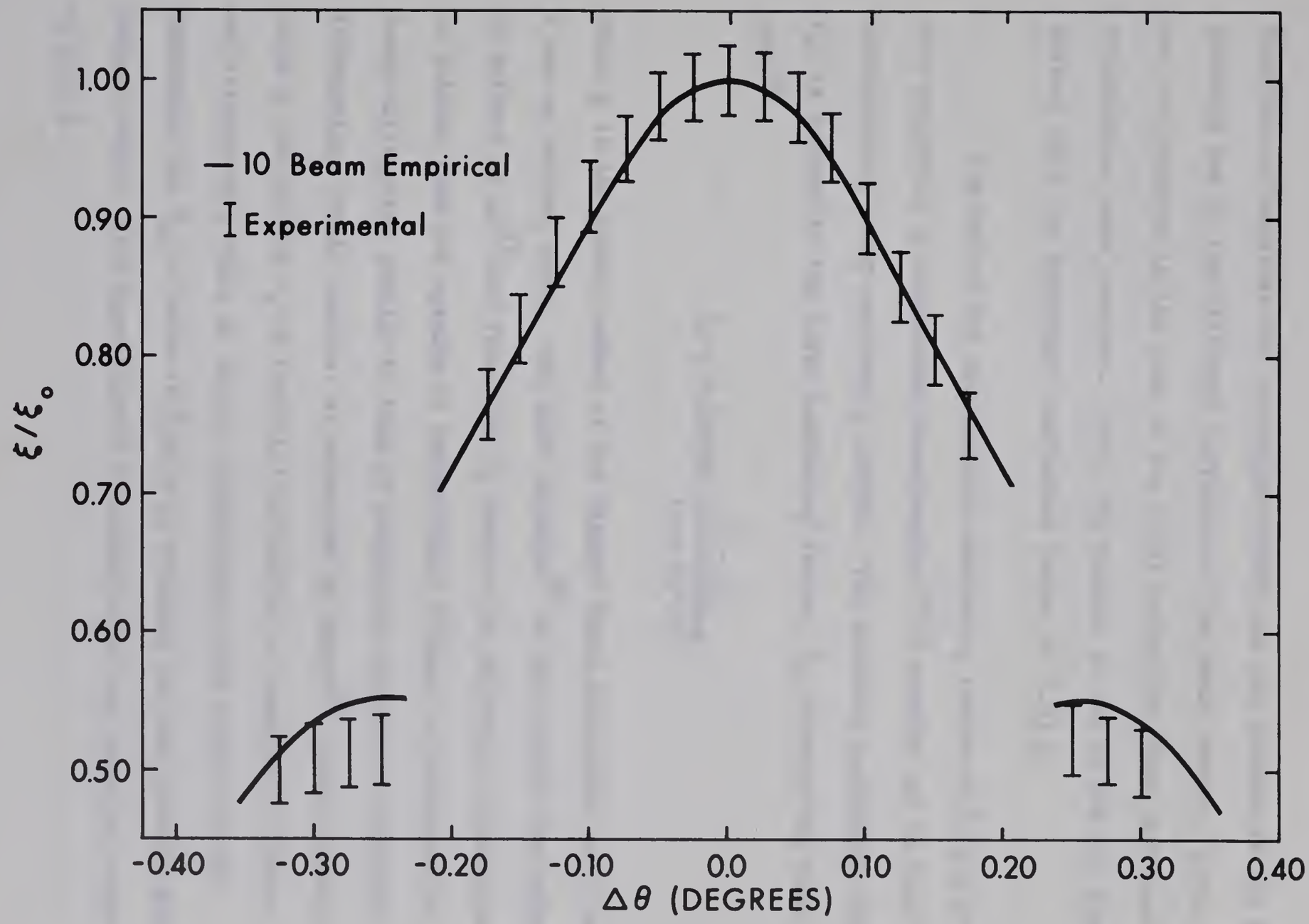
1.00
0.90
0.80
0.70
0.60
0.50
ε/ε₀
— 10 Beam Empirical
I Experimental
-0.40
-0.30
-0.20
-0.10
0.0
0.10
0.20
0.30
0.40
Δθ (DEGREES)

FIGURE 19

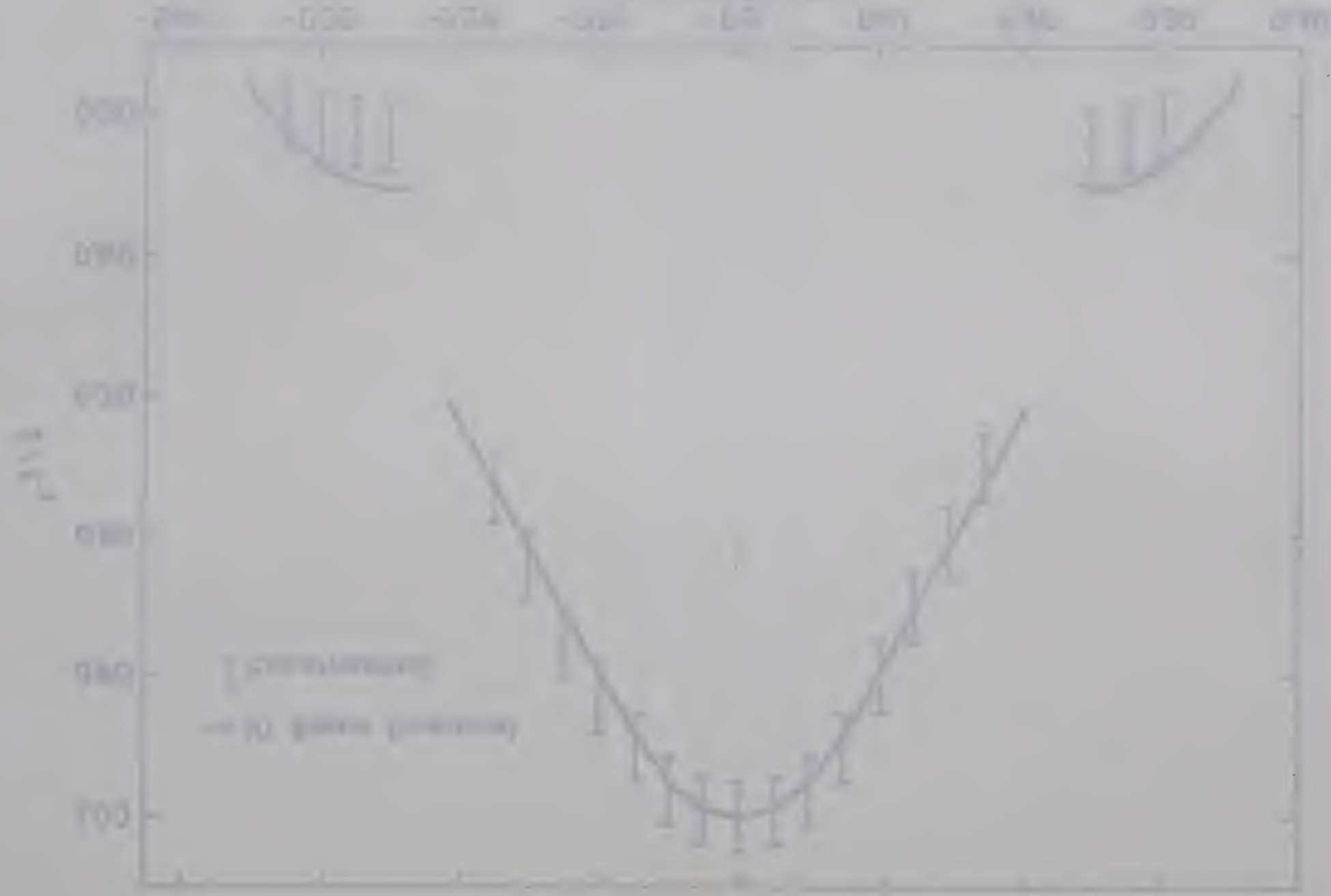

direction of negative $\Delta\theta$. A similar effect was not noticed at 152 kV, probably due to the different curvature of the Ewald sphere. Also, it was not observed in the case of the (200) reflection where different orientations were involved. Thus, the results at 100 kV are not inconsistent with the experiment scattering factor of 2.83 A.

The use of the experimental scattering factor of 2.83 A is also supported by independent measurements[31-33] carried out to find the corresponding X-ray scattering factors. The electron scattering factor, f_e, is related to the X-ray scattering factor, f_x, through the relation[28]

$$f_e = 0.023934 \frac{Z - f_x}{(\sin \theta)^2/\lambda^2},$$

where Z is the atomic number of the element being considered and θ and λ are as defined above. The most reliable[34] of the results are those of Hattori *et al.*[33] who found the f_x factors for different reflections in silicon from the spacing of Pendellösung fringes, a phenomenon in X-ray diffraction similar to that of extinction contours in electron diffraction. Their results, as corrected by Dawson[34], gave a value of $10.90 \pm .04$ for the f_x of the (111) reflection as compared to Ibers' and Vainshtein's value of 10.54. Substituting this value into the expression for f_e, a value of 2.92 A is obtained for the electron scattering factor. This agrees quite favourably with the empirical value of 2.83 A.

B. (220) Extinction Distance Measurements

The predictions of the two-beam and 7-beam approximations are so similar for this reflection that it is impossible, from the experimental results, to determine which approximation best describes the actual physical situation. The experimental results agree well with both approximations at both 100 and 152 kV. The lack of consistent results for the measurements of ξ_o for this reflection prevents correlation of these with the ξ versus $\Delta\theta$ measurements. However, Frankl[35], in his measurements of the (220) extinction distance in silicon found a value of 720 A at 100 kV for ξ_o, in excellent agreement with that predicted by the 7-beam approximation of 723 A. Thomas and Levine[36] also made measurements of the (220) extinction distance using stacking fault fringes rather than thickness contours. They obtained a value of 660 A for ξ_o at 100 kV. They did not explain the deviation from the theoretical value although they did say that it was under further investigation. Booker and Hazzledine[37] have investigated the profiles of planar defects in crystals such as stacking faults. Due to the different variables such as the defect's phase angle, the angular deviation of the reflection being considered from its Bragg condition, and absorption of the electron beams in the crystal, they concluded that "the greatest care must be taken in interpreting electron micrographs of such faults before definite conclusions can be reached." Thus, the more reliable results are those of Frankl which

are also consistent with the ξ versus $\Delta\theta$ measurements made here.

The X-ray scattering factor has also been measured for this reflection[31-33] and found to vary slightly from that given by Ibers and Vainshtein[28]. However, this variation results in only a $3\frac{1}{2}$ per cent change in the electron scattering factor. This change in scattering factor is too small to be detected here because it lies within the range of error of the present experiments.

C. Multi-Beam Effects

The effects of beams other than the two principal beams on the extinction distance can be considered for the two cases of systematic and non-systematic reflections.

The effects of systematic reflections were taken into consideration in the multi-beam calculations. In the case of the (220) reflection, the 7-beam calculations predicted values of ξ_o of 723 and 840 Angstroms at 100 and 152 kilovolts respectively as compared to the two-beam values of 760 and 890 Angstroms. However, the multi-beam predictions of the variation of ξ with $\Delta\theta$ differed from that predicted by the two-beam theory by an amount too small to detect by the measurements carried out here. Thus, for the (220) reflection the effect of the systematic reflections is to decrease ξ_o but to have a relatively small effect on the variation of ξ with $\Delta\theta$.

In the case of the (111) reflection the effects of systematic reflections were important for both ξ_o and ξ versus $\Delta\theta$. For ξ_o the 10-beam approximation predicted values of 630 and 736 Angstroms at 100 and 152 kilovolts respectively as compared to the two-beam values of 615 and 720 Angstroms. Thus, for the (111) reflection the effect of systematic reflections is a predicted increase in ξ_o as opposed to the usual decrease[38]. In the ξ versus $\Delta\theta$ measurements the two-beam theory predicts a smooth continuous variation of ξ with $\Delta\theta$, with no sharp drops. However, 3-beam calculations which included either the $(\bar{1}\bar{1}\bar{1})$ or (222) reflection were carried out and in these cases sharp drops were predicted. Moreover, these drops took place in the same range of values of $\Delta\theta$ as they were observed experimentally. As was shown earlier in Figures 12 and 13, when 10 beams were considered these drops were also predicted. However, the 3-beam approximation gave qualitative agreement with the experiment results and this agreement was only improved slightly by using a 10-beam approximation. Thus, this effect is probably associated with the "forbidden" (222) reflection in diamond structure[39] as this reflection first appears in the off-diagonal elements of the 3-beam approximations. This reflection is called "forbidden," even though it is observed in electron diffraction patterns, because its structure factor is zero. Heidenreich[39] explained the presence of a (222) reflection by double diffraction involving a pair of reflections such as (113) and $(11\bar{1})$. However, (222) reflections were observed to be present even when pairs of re-

flections such as these, which could combine to give a (222) reflection, were not. Hoerni[40] and Fujimoto[41] explained the presence of the (222) reflection by taking into account interactions between the systematic reflections including the (111) reflection. These interactions were calculated to contribute the main part of the (222) intensity even when diffracting pairs such as (113) and $(11\bar{1})$ were present. Thus, the presence of the "forbidden" (222) reflection is predicted to affect the intensity of the (111) reflection, possibly through sharp changes in extinction distance as were observed.

The effects of non-systematic reflections are much more difficult to take into consideration as there is no accurate method of determining how far these reflections are from their exact Bragg conditions for any random orientation. As was seen in Figure 14, one of the possible effects of these reflections is to change the variation of ξ with $\Delta\theta$ by introducing small sharp changes in extinction distance. Other effects were observed in making the ξ_o measurements. Here, the non-systematic reflections were found to both reduce the contrast in the image, thus, making it difficult to differentiate between the bright and dark contours, and to introduce scatter into the measured results particularly in the case of the (220) reflections at 152 kV. These observations are supported by work done by Humphreys *et al.*[42] on stacking fault fringes in gold and silicon. They carried out calculations and measurements of the effects of both systematic and non-

systematic reflections and obtained results similar to those given here.

D. Conclusions

The original purpose of the work undertaken here was to find the variation of extinction distance with angular deviation from the Bragg condition for the (111) and (220) reflections in silicon and to compare the results with the predictions of the two-beam and multi-beam approximations of the dynamical theory of electron diffraction.

In the case of the (111) reflection, a 10-beam approximation involving only systematic reflections and calculated using 2.83 A for the (111) electron scattering factor, a value obtained from ξ_o measurements, was found to be in good agreement with the experimental results. The use of this experimental scattering factor rather than the theoretical value of 3.26 A is supported by recent measurements made of the X-ray scattering factor for the same reflections. The measured X-ray factor corresponds to a value for the electron scattering factor of 2.92 A which is in close agreement with the experimental value found here. The 10-beam approximation also predicts the observed sharp drops in extinction distance, a phenomenon probably related to the "forbidden" (222) reflection. In the case of the two-beam approximation there is poor agreement with the experimental results.

In the case of the (220) reflection the predictions of the two-beam and 7-beam approximation differ only slightly and are both in good agreement with the experimental results. These ξ versus $\Delta\theta$ measurements were also in agreement with the ξ_o measurements of Frankl. Other workers have found similar results to those obtained here. Uyeda and Nonoyama[12] found agreement between the two-beam theory and experimental results for the (200) reflection in MgO. Within the range of angular deviations considered here, Sheinin[43] also found good agreement between experimental results and the predictions of the two-beam and 12-beam approximations for the (110) extinction distance in molybdenum. Thus, the variation of ξ with $\Delta\theta$ for the (111) reflection is unique among published measurements of this type in that it differs markably from the two-beam predictions. As pointed out earlier, this variation is probably due to the "forbidden" (222) reflection.

E. Suggestions For Further Work

More measurements of the variation of extinction distance with deviation from the Bragg condition for different reflections in silicon and similar measurements in other materials might be carried out to check the effect of forbidden reflections. However, it should be noted that extinction distance is basically a parameter of the two-beam theory arising out of the predicted sine squared variation for the intensity of a beam with depth in a crystal. The presence of other

reflections affects both the shape of the intensity peaks and the spacing between them. The severity of these effects depends on both the proximity of the reflections to their Bragg conditions and the energy of the incident electrons. The latter condition arises from the fact that systematic reflections would be expected to have a greater effect as the energy of the electron beam increases[11]. Thus, the use of a parameter such as extinction distance to describe a multi-beam case is open to question. Perhaps, a more accurate method of checking the various theories is to compare the shape of the theoretical depth intensity profiles of a beam with the actual observed shape in the densitometer traces. This approach would be especially useful in the regions of complex periodicity. However, in making theoretical predictions of the shape of contours it is necessary to include the effects of absorption. Such effects are not yet completely understood.

REFERENCES

1. M. Knoll and E. Ruska, Ann. d. Physik 12, 607 (1932).
2. B. von Borries and E. Ruska, Naturwiss. 28, 366 (1940).
3. J. Hillier and R.F. Baker, Phys. Rev. 61, 722 (1942).
4. R.D. Heidenreich, Phys. Rev. 62, 291 (1942).
5. H. Boersch, Zeit. f. Physik 121, 746 (1943).
6. E. Kinder, Naturwiss. 31, 149 (1943).
7. R.D. Heidenreich and L. Sturkey, J. Appl. Phys. 16, 97 (1945).
8. H.A. Bethe, Ann. D. Physik 87, 55 (1928).
9. H. Hashimoto, J. of Appl. Phys. 35, 277 (1964).
10. G. Dupouy, F. Perrier, R. Uyeda, R. Ayroles, and A. Mazel, J. Microsc. 4, 429 (1965).
11. M.J. Goringe, A. Howie, and M.J. Whelan, Phil. Mag. 14, 217 (1966).
12. R. Uyeda and M. Nonoyama, Japan. J. Appl. Phys. 4, 498 (1965).
13. C.H. MacGillavry, Physica 7, 329 (1940).
14. R.D. Heidenreich, J. Appl. Phys. 20, 993 (1949).
15. R.D. Heidenreich, Fundamentals of Transmission Electron Microscopy (Interscience Publishers, New York, 1964), p. 202.
16. L. Sturkey, Proc. Phys. Soc. 80, 321 (1962).
17. A. Howie and M.J. Whelan, Proc. Roy. Soc. A263, 217 (1961).
18. F. Fujimoto, J. Phys. Soc. Japan 14, 1558 (1959).
19. H. Niehrs, Z. Phys. 156, 446 (1959).

20. H. Hashimoto, A. Howie, and M.J. Whelan, Proc. Roy. Soc. A269, 80 (1962).

21. K. Fujiwara, J. Phys. Soc. Japan 16, 2226 (1961).

22. S.S. Sheinin, Rev. Sci. Instr. 37, 232 (1966).

23. E.S. Greiner, J.A. Gutowski, and W.E. Ellis, J. Appl. Phys. 32, 2489 (1961).

24. A.V. Sandulova, P.S. Bogoyavlenskii, and M.I. Dronyuk, Fiz. Tvend. Tela 5, 2580 (1963) [English transl: Soviet Phys.--Solid State 5, 1883 (1964)].

25. R.W. Wagner, W.C. Ellis, K.A. Jackson, and S.M. Arnold, J. Appl. Phys. 35, 2993 (1964).

26. H. Schäfer and B. Morcher, Z. Anorg. Allgem. Chem. 290, 279 (1957).

27. E.S. Wajda and R. Glang, Met. Soc. Conf. 12, 229 (1961).

28. J.A. Ibers and B.K. Vainshtein, International Crystallographic Tables, Vol. III, Tables 3.3.3A(1) and A(2), (Kynoch Press, Birmingham, 1962).

29. J.A. Ibers, Acta Cryst. 11, 178 (1958).

30. J.A. Ibers, J. Phys. Soc. Japan 17, Suppl. B-II, 4 (1962).

31. S. Göttlicher and E. Wölfel, Z. Elektrochem. 63, 891 (1959).

32. J.J. DeMarco and R.J. Weiss, Phys. Rev. A, 137, 1869 (1965).

33. H. Hattori, H. Kuriyama, J. Katagawa, and N. Kato, J. Phys. Soc. Japan 20, 988 (1965).

34. B. Dawson, Proc. Roy. Soc. A298, 379 (1967).

35. D.R. Frankl, J. of Appl. Phys. 35, 217 (1964).

36. G. Thomas and E. Levine, phys. stat. sol. 11, 81 (1965).

37. G.R. Booker and P.M. Hazzledine, Phil. Mag. 15, 523 (1967).

38. P.B. Hirsch, A. Howie, R.B. Nicholson, D.W. Pashley, and M.J. Whelan, Electron Microscopy of Thin Crystals (Butterworths, London, 1965), p. 280.

39. R.D. Heidenreich, Phys. Rev. 77, 271 (1950).

40. J.A. Hoerni, Phys. Rev. 102, 1534 (1956).

41. F. Fujimoto, J. Phys. Soc. Japan 15, 1022 (1960).

42. C.J. Humphreys, A. Howie, and G.R. Booker, Phil. Mag. 15, 507 (1967).

43. S.S. Sheinin, phys. stat. sol. 21, 247 (1967).